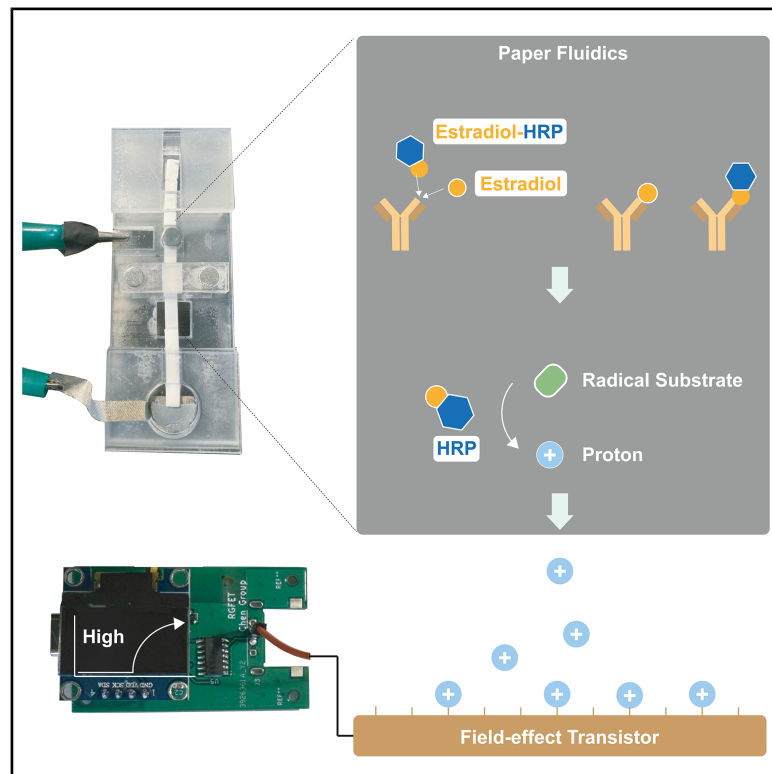


Radical-mediated electrical enzyme assay for estradiol: Toward point-of-care diagnostics

Graphical abstract



Authors

Hyun-June Jang (현준장),
Hyou-Arm Joung (효암정), Xiaoao Shi, ...,
Kiang-Teck Jerry Yeo, Jun Huang,
Junhong Chen

Correspondence

junhongchen@uchicago.edu

In brief

Jang et al. present a low-cost, rapid radical-mediated electrical enzyme assay (REEA) integrated with a paper-fluidic system and a handheld field-effect transistor (FET) reader. This platform enables biomarker quantification with a detection limit of 146 fg/mL and an accuracy of $r^2 = 0.963$ across a range of 19–4,551 pg/mL, with results in under 10 min and a cartridge cost of \$0.55 per test.

Highlights

- Proposes a radical-mediated electrical enzyme assay method for immunoassays
- Integrates electronics and paper fluidics for point-of-care tests
- Costs only \$0.55 per test with results in 10 min
- Achieves 146 fg/mL detection limit for estradiol with precision in clinical samples



Develop

Prototype with demonstrated applications in relevant environment

Jang et al., 2025, Device 3, 100807
September 19, 2025 © 2025 The Author(s).
Published by Elsevier Inc.
<https://doi.org/10.1016/j.device.2025.100807>

Article

Radical-mediated electrical enzyme assay for estradiol: Toward point-of-care diagnostics

Hyun-June Jang (현준장),^{1,2,10} Hyou-Arm Joung (효암정),^{3,10} Xiaoxiao Shi,^{1,2} Rui Ding,^{1,2} Justine Wagner,^{4,5,6} Erting Tang,¹ Wen Zhuang,^{1,2} Byunghoon Ryu (병훈류),⁷ Guanmin Chen,⁸ Kiang-Teck Jerry Yeo,^{8,9} Jun Huang,¹ and Junhong Chen^{1,2,11,*}

¹Pritzker School of Molecular Engineering, University of Chicago, Chicago, IL 60637, USA

²Chemical Sciences and Engineering Division, Physical Sciences and Engineering Directorate, Argonne National Laboratory, Lemont, IL 60439, USA

³Kompass Diagnostics Inc., Chicago, IL 60651, USA

⁴School of Chemistry and Biochemistry, Georgia Tech Polymer Network, Georgia Institute of Technology, Atlanta, GA 30332, USA

⁵School of Materials Science and Engineering, Georgia Tech Polymer Network, Georgia Institute of Technology, Atlanta, GA 30332, USA

⁶Center for Organic Photonics and Electronics, Georgia Tech Polymer Network, Georgia Institute of Technology, Atlanta, GA 30332, USA

⁷Department of Mechanical Engineering, Inha University, Incheon 22212, Republic of Korea

⁸Department of Pathology, The University of Chicago, Chicago, IL 60637, USA

⁹Pritzker School of Medicine, The University of Chicago, Chicago, IL 60637, USA

¹⁰These authors contributed equally

¹¹Lead contact

*Correspondence: junhongchen@uchicago.edu

<https://doi.org/10.1016/j.device.2025.100807>

THE BIGGER PICTURE Management of chronic health conditions—such as cardiovascular and reproductive disorders—depends on the frequent and reliable monitoring of specific biomarkers. This is achieved through clinic visits or mail-in tests, where blood samples are analyzed in centralized laboratories. Current point-of-care technologies, which rely on colorimetric immunoassays, lack the sensitivity and precision required to detect biomarkers at trace levels. While advanced spectroscopic methods offer high analytical performance, their complexity, bulkiness, and cost make them impractical for decentralized or at-home use. To address these limitations, we have developed a low-cost, lab-quality diagnostic platform that integrates a radical-mediated electrical enzyme assay (REEA) with paper-based microfluidics and an affordable handheld reader. This system detects estradiol, a hormone associated with women's reproductive care, and offers the potential for accessible and accurate biomarker monitoring.

SUMMARY

The diagnosis and prognosis of many conditions such as cardiovascular, neurodegenerative, and reproductive disorders often require repeat monitoring of small molecules, proteins, hormones, or other biomarkers with a high analytical sensitivity. We developed a radical-mediated electrical enzyme assay (REEA) in a paper-based fluidic cartridge (\$0.55/test) with a handheld reader utilizing field-effect transistors to measure estradiol (E2), a key hormone in reproductive care. The system demonstrated a detection limit of 146 fg/mL, a coefficient of variation below 9.2%, and an accuracy of 0.963 across 19–4,551 pg/mL in clinical plasma samples, with results delivered in under 10 min. The REEA method presents a high-sensitivity electrochemical transducing system and can be used to detect other high-sensitivity biomarkers, including cardiac troponin and tau proteins associated with Alzheimer's disease.

INTRODUCTION

The diagnosis, prognosis, and treatment of various health conditions, such as cardiovascular, neurodegenerative, and reproductive disorders, rely on long-term assessment of biomarkers.^{1–3} For example, infertility treatments such as *in vitro* fertilization require frequent monitoring of plasma estradiol (E2) levels to

achieve optimal outcomes.^{4–6} Such frequent testing imposes time, cost, and energy burdens^{7,8} on patients and capacity constraints for providers.⁹ In the evolving healthcare landscape marked by rising costs, increased demand for convenient care delivery, workforce shortages, and limited provider capacity, there is a growing need for accurate, cost-effective home-based diagnostic solutions.

Monitoring E2 is crucial for women's health; elevated levels¹⁰ are linked to conditions such as fibroids, endometriosis, and an increased cancer risk, while diminished levels¹¹ may indicate ovarian insufficiency or menopause, impacting fertility, physical, mental, and reproductive health. Furthermore, extremely low concentrations of E2, under a few pg/mL, typically signify hypoestrogenism,¹² a condition associated with severe health complications such as osteoporosis,¹² cardiovascular issues,¹³ cognitive decline,¹⁴ mood disturbances,¹⁴ and an increased risk of autoimmune diseases.¹⁵ However, hormone assays for estrogen usually need lab-based chemiluminescence immunoassays (CLIA) due to its low and variable concentration during pregnancy (20–20,000 pg/mL) and susceptibility to biomolecular interference.¹⁶ This complexity presents significant challenges in adapting current analytical methods¹⁷ to at-home testing environments.

For at-home E2 test solutions, incorporating CLIA techniques into portable devices is fraught with challenges due to the unstable nature of reagents, necessitating sophisticated microfluidic systems and optical detectors that escalate both complexity and cost.¹⁸ Additionally, optical-based point-of-care (POC) estradiol detection¹⁹ suffers from an insufficient limit of detection (LOD), making them unsuitable for diagnostics purposes. Meanwhile, mail-in tests, which involve self-collecting finger-prick blood samples and sending them to labs for chemiluminescence analysis, provide a greater accuracy but rely on lab processing, which can delay crucial fertility treatment decisions. Electrical detection through field-effect transistor (FET) biosensors offers rapid and sensitive detection at fg/mL levels^{20–23} yet commercialization is hindered by complex fluidic controls needed to manage sample matrix interference^{24,25} and Debye length (λ_D) constraints.^{21,24} Additionally, maintaining the necessary wet interface for FETs raises issues of fluid leakage and damage, complicating commercial viability. Furthermore, achieving consistent control of batch-to-batch and device-to-device variability is crucial for broad market adoption.²⁴

In clinical settings, the enzyme horseradish peroxidase (HRP) catalyzes substrate transformations, generating optical signals directly linked to analyte concentrations.²⁶ However, by repurposing HRP-substrate interactions for electrical detection, protons generated during the reaction can be quantified by a FET, with proton count correlating to analyte concentration. This approach, termed "radical-mediated electrical enzyme assay" (REEA), overcomes sample matrix interference, allows the direct use of human plasma samples, enables a simplified fluidic design, and maintains high sensitivity and a miniaturized device.

Here, we present a diagnostic platform that integrates REEA with a paper-based fluidic system²⁷ and a handheld FET reader, capable of measuring E2 at concentrations below pg/mL. The FET quantifies protons generated within the paper fluidics cartridge by the REEA system, correlating the proton count with the concentration of target analytes. As a proof-of-concept, E2 was measured with a LOD of 146 fg/mL under E2-spiked buffer condition and a coefficient of variation (CV) below 9.2% (clinically relevant range of E2: 1 pg/mL to 5 ng/mL). The assay utilized a cartridge costing \$0.55 per test (Table S1). The system demonstrated a strong correlation ($r^2 = 0.963$) across a measuring range of 19 to 4,551 pg/mL for 23 plasma samples, with a standard error of estimate (Sy/x) of 0.15 in a logarithmic regression analysis. These re-

sults are comparable with those obtained with an FDA-cleared clinical immunoassay on the Cobas e801 analyzer, indicating high accuracy. Screening 14 phenolic compounds interacting with HRP identified halogenated phenolic substrates—such as 4-fluorophenol (FP), 4-iodophenol (IP), 4-chlorophenol (CP), and 4-bromophenol (BP)—as the most effective for REEA. Additionally, the REEA cartridge was equipped with an enzymatic choline oxidase (ChOx)-based system for automated hydrogen peroxide (H_2O_2) generation. This technology can help enable early detection and monitoring of various health conditions, including hormonal imbalances, metabolic disorders, chronic diseases, and infectious diseases.

RESULTS

Detection platform and working mechanism of REEA

The integration of FET technology with paper fluidics and the REEA system offers a low-cost, accurate, and accessible solution for potentially using it as an at-home clinical test. Figure 1A depicts the handheld FET reader device (dimensions 2.5 × 4 cm) and the paper-based immunoassay cartridge for E2 detection. The basic electrical properties of the FET used in all experiments are shown in Figure S1. To operate, the clinical sample is first mixed with an optimized running buffer that facilitates movement of the mixed sample along the test strip, followed by a 15-min incubation period (Figure 1B). Following incubation, the cartridge, which includes the sensing electrodes such as indium tin oxide (ITO) and reference electrodes, is electrically connected to designated terminals on the handheld device (Figure S2). A total 300 µL of mixture of plasma and reagents is then injected into the cartridge, and the device begins real-time measurement of the signal over a 10-min period.

HRP, an enzyme commonly used in analytical techniques to convert substrates into optical signals (Figure 1C), is repurposed in the REEA system to convert aromatic substrates into radical forms, generating protons^{28,29} (Figure 1D). HRP, which contains an Fe(IV) oxyferryl center, undergoes oxidation by H_2O_2 , leading to the formation of compound I.³⁰ Compound I then interacts with a phenol compound (PhOH) at its active site, generating and releasing a phenolic free radical and a proton into the medium. The reaction produces compound II, which further reacts with another phenol molecule, releasing an additional proton. These protons, which correlate with the concentration of the target analyte, serve as the signal in the REEA system and are quantified by an ion-sensitive FET (Figure 1E). The pH sensitivity of the ITO electrode was measured using a remote-gate FET (RGFET) setup^{25,31} with a semiconductor analyzer and standard Ag/AgCl reference electrode (Figure S3A). Figure S3B shows the transfer curve shifts as a function of pH, exhibiting parallel shifts without any change in curve shape. This behavior corresponds to a proton-specific Nernstian response of 52.4 mV/pH with an r^2 of 0.998 (Figure S3C), calculated based on threshold voltage (V_{th}) shifts across different pH levels. Additionally, no interference from variations in the surface area of the testing solution on the ITO was observed, owing to the high input impedance of the FET³² (Figure S3D).

A set of phenolic and aniline compounds with a wide range of pKa values (Figure 2A), including 2,4,6-trimethoxyphenol

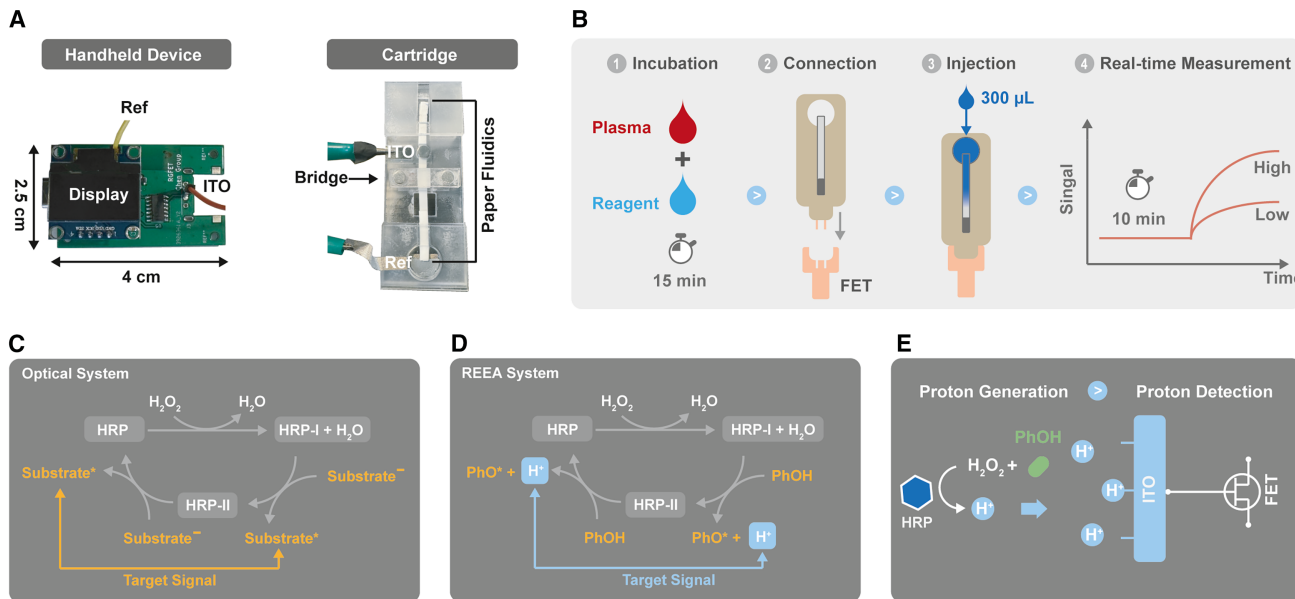


Figure 1. Measurement system and REEA mechanism

(TMYP), 2,4,6-trimethylphenol (TMLP), 4-methoxyphenol (MP), FP, IP, CP, BP, 2,4,6-trichlorophenol (TCP), *p*-anisidine (AD), *p*-toluidine (T), 4-fluoroaniline (FA), *o*-phenylenediamine (OPD), 2,4,6-trimethylaniline (TMYA), and 4-chloroaniline (CA), was screened to identify the optimal substrate for REEA in the solution phase. The screening was performed using the RGFET setup with a semiconductor analyzer and a standard Ag/AgCl reference electrode (Figure S4A). Different degrees of shifts in V_{th} were observed in Figure 2B by the reaction between HRP, H_2O_2 , and each substrate (Figures S4B and S4C). Without H_2O_2 and HRP (Figure S4D), and with either H_2O_2 (Figure S4E) or HRP (Figure S4F) alone, changes in V_{th} were minimal for all substrates.

The detection signal, defined as the difference in V_{th} between the HRP/ H_2O_2 /substrate mixture and the substrate-only condition, reveals that halogenated phenolic compounds—specifically FP, IP, CP, and BP—generated the most substantial signals (Figure 2C). The oxidation of these compounds results in the release of halogenated ions,^{33,34} leading to the formation of hydrofluoric acid, hydroiodic acid, hydrochloric acid, and hydrobromic acid, respectively (inset of Figure 2B). These strong acids contribute to a significant reduction in V_{th} . Density functional theory simulations³⁵ conducted to calculate changes in enthalpy (ΔH) and Gibbs free energy (ΔG) support that proton generation is favorable for these halogenated ions (Figure 2D; Table S2). FP was selected for subsequent experiments due to its high sensitivity, relative safety, commercial availability, and good solubility. Compared with IP, CP, and BP, FP is easier to handle with lower toxicity and demonstrates greater applicability in practical experimental settings. These combined advantages made FP the most appropriate choice for optimizing the REEA platform.

The REEA system addresses λ_D issues, which are challenges in FET biosensors that limit their ability to detect charged biomolecules in concentrated biological fluids. In particular, conventional FET biosensors exhibit a low sensing margin when the spatial distribution of protein charges extends beyond the λ_D value.^{31,36} Given that the λ_D in body fluids is less than 1 nm—far shorter than biomolecules such as antibodies, which are typically 10–15 nm in size—conventional label-free immune-FET biosensors frequently require washing or buffer exchange steps. These steps are necessary to measure changes in surface potential caused by biomolecule interactions and to effectively manage λ_D issues.

The REEA system has demonstrated V_{th} shifts in concentrated testing environments, such as in both 1× phosphate-buffered saline (PBS) (Figure S5A) and plasma (Figure S5B), with HRP concentrations ranging from 10 pg/mL to 1 μ g/mL (Figure 2E). This suggests the applicability of body fluids as testing solutions, utilizing a simple fluidic system for the REEA. The transfer curves exhibit parallel shifts during the HRP-substrate reaction, without changes in shape, even in plasma samples (Figure S5C). This indicates that the surface potential changes are caused by the HRP-substrate reaction, without interference or nonspecific signaling. The maximum signal window, measured from control to 1 μ g/mL HRP, was determined to be approximately 0.37 V in PBS and 0.32 V in plasma. However, at HRP concentrations exceeding 10 μ g/mL, a reversal in V_{th} was observed for both PBS and plasma, suggesting a potential saturation point in the REEA signal. This reversal is likely due to HRP inactivation (Figures S5A and S5B), where the disruption of the heme macrocycle by phenoxyl radical attacks impairs its catalytic function.³⁷

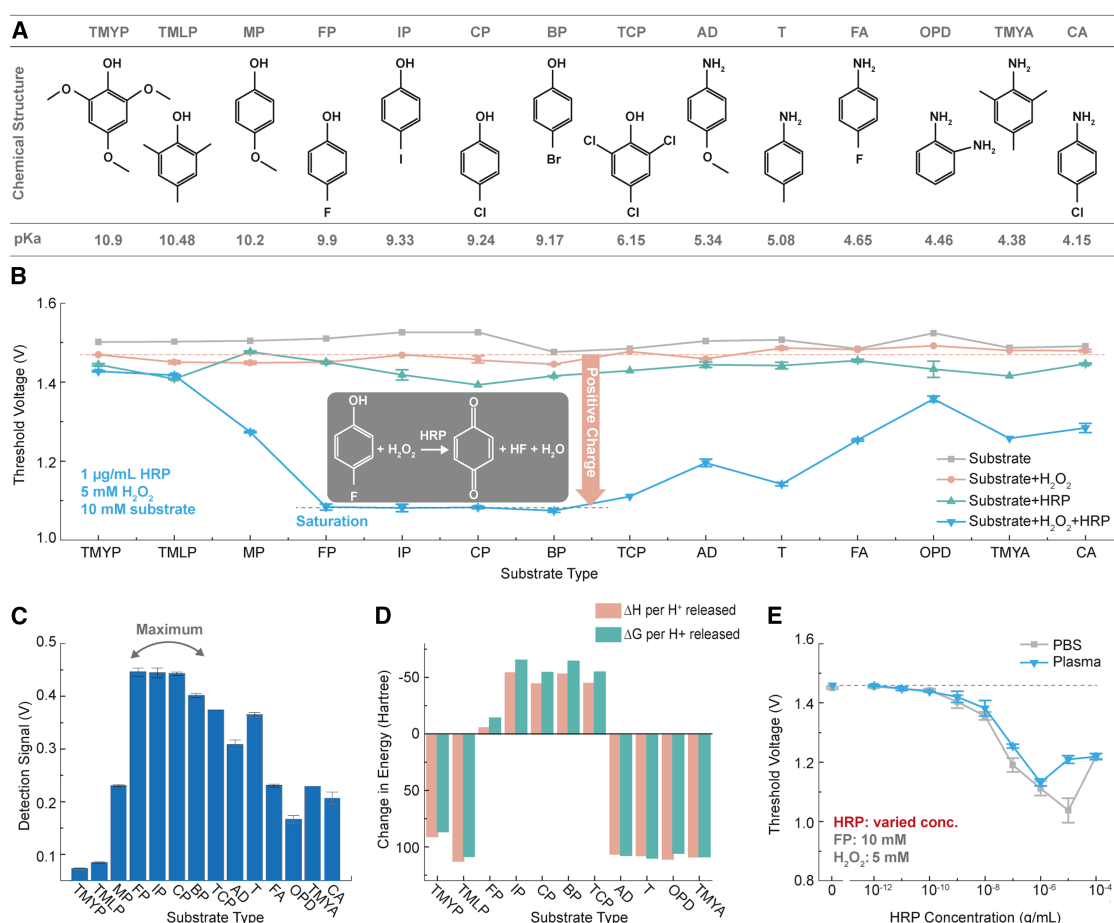


Figure 2. Fundamental understanding in REEA

- (A) The chemical structures of the phenolic compounds tested for the REEA system.
- (B) The distribution of V_{th} versus substrate reacted with HRP and H_2O_2 , including controls with substrate alone, substrate with H_2O_2 but no HRP, and substrate with HRP but no H_2O_2 .
- (C) Detection signals as a function of substrate type.
- (D) Changes in ΔH and ΔG simulated by density functional theory for each substrate type.
- (E) V_{th} versus HRP concentration at 10 mM FP and 5 mM H_2O_2 diluted in either PBS or plasma. Error bars in Figures 2B, 2C, and 2E represent standard error of the mean.

Validation of RGFET in the handheld reader system

An affordable handheld reader system constitutes the other component for translating the REEA system into a practical clinical testing tool. The measurements performed using the handheld reader need to be validated using the semiconductor analyzer measurements as demonstrated above.

The real-time change in the drain current of the FET, measured at a constant gate voltage of 2 V and drain voltage of 3 V in the handheld device system, reflects alterations in surface potential on the ITO and is converted into an output voltage (V_{out}) (Figure S6A). V_{out} is primarily derived from the voltage drop across a fixed resistor at the drain terminal, measured through differential voltage amplification using an operational amplifier (op-amp) with a 4 \times voltage gain. Since V_{out} is proportional to the drain current, it represents the drain current multiplied by a constant resistance.

The real-time pH sensitivity (Figure S6B), measured as the V_{out} change using the handheld FET reader with the standard Ag/

AgCl reference electrode and ITO in response to the pH of the testing solution, exhibited an amplified response of 212 mV/pH, which is 4.04 times higher than the pH sensitivity measured from the V_{th} using the semiconductor analyzer in Figure S3C. This enhancement is attributed to the built-in op-amp in the handheld device. The test result demonstrated 99.4% accuracy (Figure S6C) and high stability with negligible drift (Figure S6D).

Potential interferences caused by various paper materials, including nitrocellulose (NC) membrane, cotton linter pad, cellulose filtration paper, two glass fiber pads, and polysulfone membrane, inserted between the ITO electrode and the solution (Figure S7A), were found to be insignificant. This was confirmed using the handheld reader device and a standard Ag/AgCl reference electrode. That is, the V_{out} signal remained stable to the pH of the buffer solution, regardless of the paper type connected to the ITO electrode (Figure S7B). The handheld FET reader's detection performance, as evaluated by the HRP-FP reaction

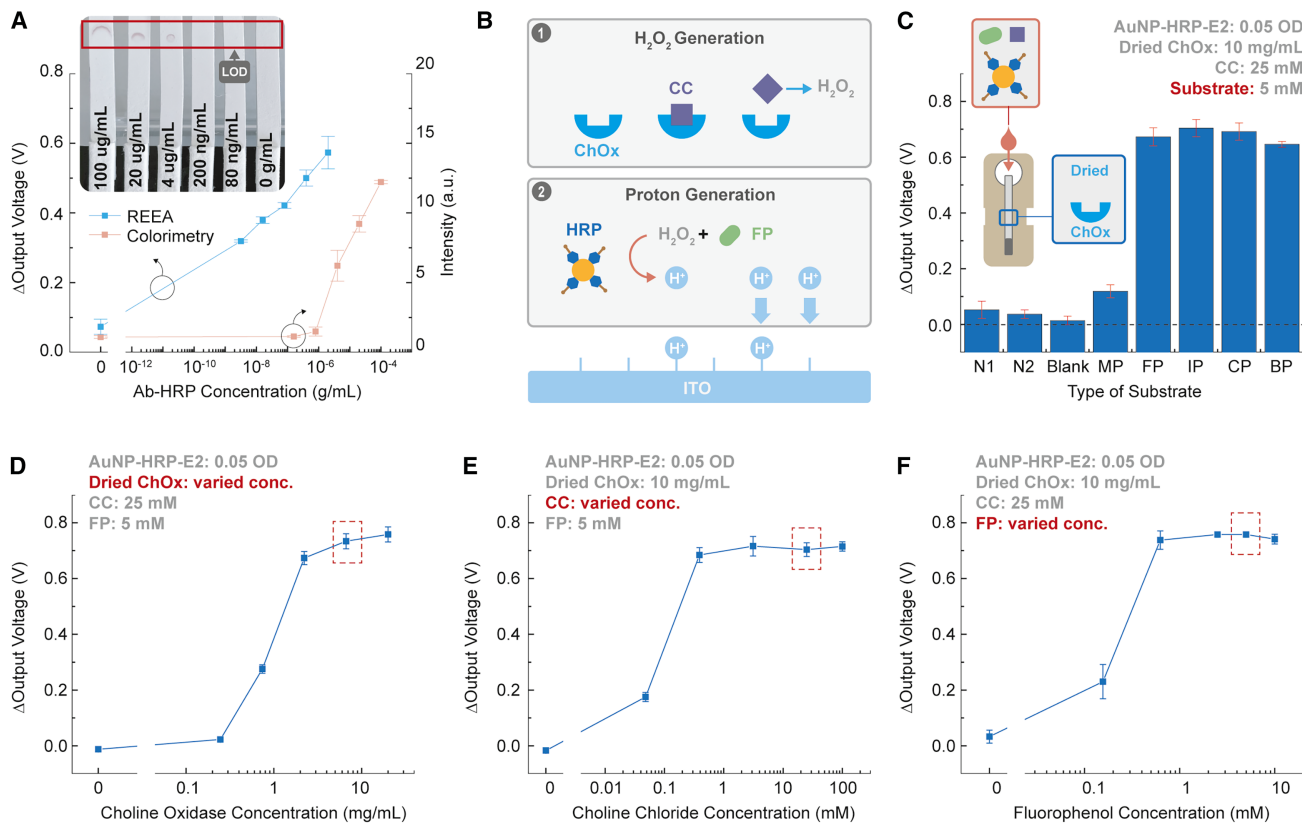


Figure 3. REEA system within paper fluidics

(A) Signal comparison from paper fluidics strips spotted with anti-E2 antibodies (0–100 µg/mL), analyzed using the REEA system and the handheld device, alongside colorimetry. The inset shows images of paper fluidics strips characterized using TMB.

(B) Schematic of the automated H_2O_2 generation system, illustrating the interaction between ChOx and CC and the subsequent HRP-FP reaction.

(C) ΔV_{out} of paper fluidics dried with ChOx and analyzed with AuNP-HRP-E2, CC, and each REEA substrate. The inset shows components of the cartridge and the testing solution.

(D) ΔV_{out} of paper fluidics dried with varying concentrations of ChOx (for testing solution: AuNP-HRP-E2 at 0.05 OD, CC at 25 mM, and FP at 5 mM).

(E) ΔV_{out} of paper fluidics dried with 10 mg/mL ChOx in response to different CC concentrations (for testing solution: AuNP-HRP-E2 at 0.05 OD, and FP at 5 mM).

(F) ΔV_{out} of paper fluidics dried with 10 mg/mL ChOx in response to varying FP concentrations (for testing solution: AuNP-HRP-E2 at 0.05 OD, and CC at 25 mM). Error bars in Figures 3A, 3C, 3D, 3E, and 3F represent standard error of the mean.

in solution phase (Figure S8A), closely matched that of a semiconductor analyzer (Figure S8B).

A copper (Cu) reference electrode was used as an alternative to the standard Ag/AgCl reference electrode in the miniaturized cartridge system (Figure S9). The Cu reference electrode demonstrated pH sensitivity comparable with that of the Ag/AgCl electrode (Figure S9B). The signal trend in HRP-FP reaction measured by the Cu electrode (Figure S9C) was comparable with the signal from the Ag/AgCl electrode (Figure S9D), as shown in Figure S9E. The ITO-Cu electrode maintained a stable V_{out} over 5,000 s after reaching a specific value corresponding to the HRP-substrate reaction, with an insignificant drift (Figure S10).

Validation of the REEA system within paper fluidics

To demonstrate the high sensitivity of the REEA system within the paper fluidic system, the LOD for both optical and REEA systems was compared with a conventional lateral flow assay format. From this section onward, all measurements were per-

formed using the handheld reader device and a Cu reference electrode. The NC membrane, dried with varying concentrations of anti-E2 antibody, was tested by adding anti-mouse IgG-HRP. After the washing step, the strips were imaged using a tetramethylbenzidine (TMB) solution, producing distinct bands corresponding to different anti-E2 antibody concentrations (inset of Figure 3A). The LOD measured by colorimetry was estimated to be 80 ng/mL (Figure 3A). However, when the same paper fluidics setup was characterized using the HRP-FP reaction, the LOD was determined to be at least 1,000 times lower than that achieved through colorimetry (Figures 3A and S11).

To enhance the HRP signal for target analyte binding, gold nanoparticles (AuNPs) were conjugated with estradiol-HRP (E2-HRP), designed for the E2 detection system. The AuNP-HRP-E2 conjugates were dried onto the NC membrane and tested across a concentration range of 0–10 optical density (OD at 525 nm) (Figure S12A). The HRP-FP reaction produced an intense signal even at a low AuNP-HRP-E2 concentration of 0.025 OD (Figure S12B), demonstrating that AuNPs conjugated

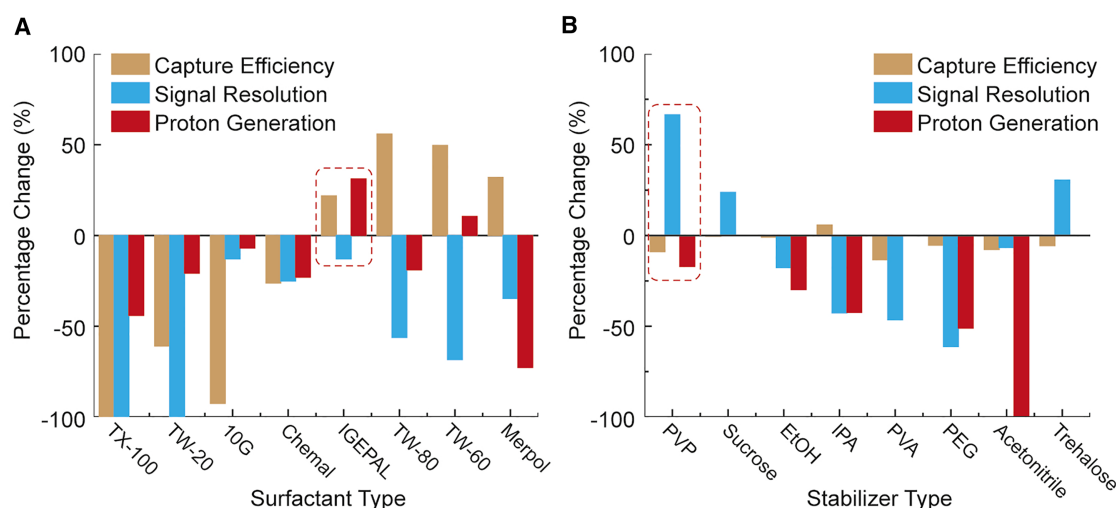


Figure 4. Optimization of running buffer

Capture efficiency, signal resolution, and proton generation efficiency, with (A) each surfactant and (B) stabilizer mixed into a 2% BSA solution.

with HRP function effectively within the REEA system, as also shown in *Figure 3A*.

H_2O_2 , a key component in REEA, is unstable under ambient conditions, making automated H_2O_2 generation upon sample injection critical for ensuring long-term stability and commercial scalability of the system. This was achieved through the interaction between ChOx and choline chloride (CC) in the signal zone (*Figure S2*) of the cartridge. The ChOx-CC enzymatic reaction produces H_2O_2 , which triggers the secondary enzymatic reaction between HRP and the REEA substrate (*Figure 3B*). To validate this automated H_2O_2 generation system, ChOx was dried onto the NC membrane (inset of *Figure 3C*) and tested with an injected solution containing AuNP-HRP-E2 conjugate (0.05 OD), 25 mM CC, and 10 mM of each substrate identified through screening (*Figure 2*). The resulting REEA signals were in agreement with those observed in *Figure 2B*, while negligible signals were detected in negative control 1 (N1: no substrate, with HRP and CC), negative control 2 (N2: no substrate and HRP, with CC), and the blank control (buffer only). These results confirm the system's specificity and functionality, demonstrating its effectiveness in automating H_2O_2 generation for the REEA process.

Using the same testing setup as shown in *Figure 3C*, the concentration of ChOx dried on the NC membrane was optimized for the REEA system to ensure sufficient H_2O_2 production without compromising the REEA signal (*Figure 3D*). A ChOx concentration above 2 mg/mL resulted in a saturated response (*Figure S13A*), with 10 mg/mL selected as the optimal concentration for subsequent experiments. Similarly, the concentration of CC in the injected solution was varied while maintaining constant levels of dried ChOx (10 mg/mL), AuNP-HRP-E2 (0.05 OD), and FP (5 mM) (*Figures 3E* and *S13B*). Saturation was observed at CC concentrations above 1 mM, with 25 mM chosen as the optimal concentration. Finally, FP concentration was optimized under the conditions established in *Figures 3D* and *3E*. FP concentrations above 0.5 mM led to signal saturation, and 5 mM was

selected as the optimal concentration for further experiments (*Figures 3F* and *S13C*).

Surfactants for the testing solution were screened in *Figure 4A* by evaluating the 24 different surfactants listed in *Table S3*. The investigation focused on E2 capture efficiency, signal resolution, and proton generation efficiency, with each surfactant mixed into a 2% BSA in 1× PBS solution. IGEPAL was selected for its ability to increase E2 capture efficiency by 21.8% and proton generation efficiency of REEA system by 31.06%, while maintaining robust baseline control with a CV of 3.04%. The CV, which measures the relative variability of data, was calculated by dividing the standard deviation by the mean. However, IGEPAL slightly reduced the signal resolution by 12.93%, where signal resolution is defined as the difference between the signal for a sample with no free E2 and the signal for the same solution spiked with 1 ng/mL of E2. (*Table S3*). To mitigate this, stabilizer components were screened in *Figure 4B*, leading to the selection of 2.5% PVP, which enhanced the signal resolution by 66.49%. The final optimized reagent comprised 2% BSA, 0.2% IGEPAL, and 2.5% PVP.

REEA cartridge for E2 detection

The cartridge designed for E2 detection is divided into three primary zones: detection, bridge, and signal (*Figure 5A*). The process begins with the mixing of a plasma sample with AuNP-HRP-E2 (0.1 OD), E2 antibody, CC (25 mM), and FP (5 mM) (step 1). This mixture is incubated for 15 min to allow the competitive reaction to occur within the testing solution (step 2). Due to its smaller size, free E2 has a higher binding affinity for the antibodies compared with the larger AuNP-HRP-E2 conjugates. After injection of the incubated sample into the main chamber, the sample flows through the detection zone—functionalized with secondary antibodies—where E2 antibodies bound to either AuNP-HRP-E2 or free E2 are captured. Within the detection zone of the cartridge strip, E2 antibodies—bound either to AuNP-HRP-E2 or free E2—are captured by secondary antibodies immobilized in this zone (step 3). The unbound

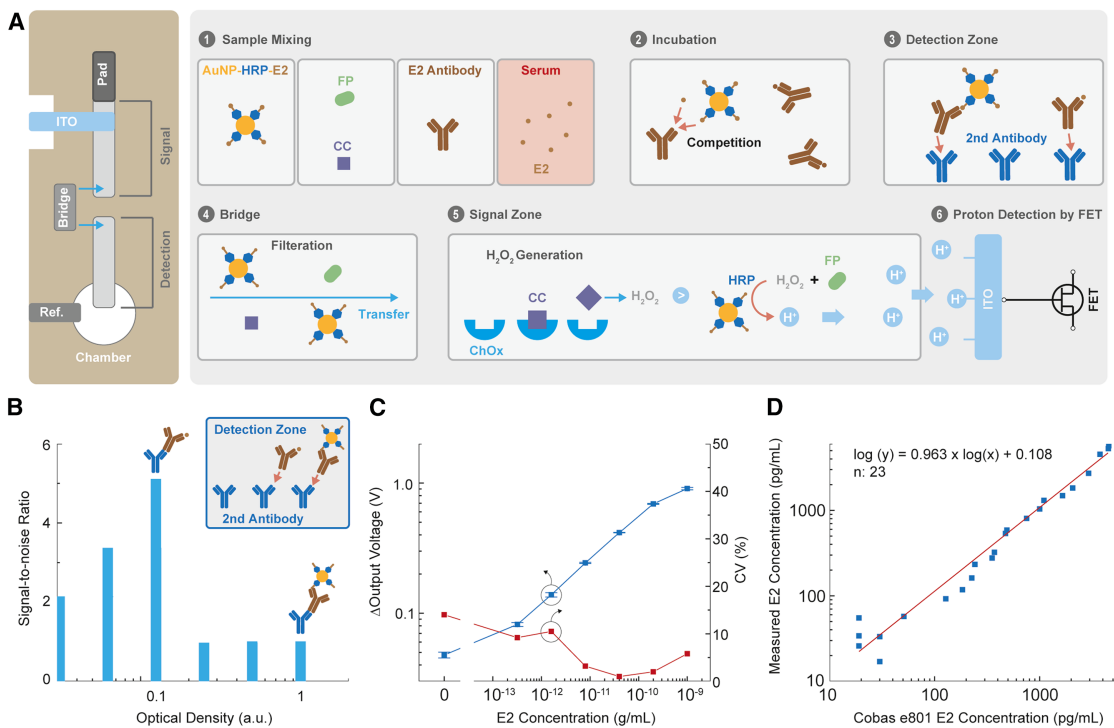


Figure 5. REEA cartridge

(A) Schematic of REEA cartridge operation with incubation method.

(B) SNR as a function of AuNP-HRP-E2 conjugate concentration in testing samples.

(C) ΔV_{out} and CV values in response to spiked E2 concentrations ranging from 328 fg/mL to 1 ng/mL.

(D) Comparison of E2 testing results obtained from the REEA system and an FDA-cleared clinical laboratory immunoassay (Cobas e801, n = 23). Error bars in Figure 5C represent standard error of the mean.

AuNP-HRP-E2 conjugates, together with CC and FP, then migrate across the bridge zone (step 4) to the signal zone (step 5), where ChOx is immobilized. In the signal zone, the first enzymatic reaction occurs between CC and ChOx, producing H₂O₂. This H₂O₂ initiates a second enzymatic reaction between HRP on the AuNP conjugate and FP, generating protons. These protons induce surface potential changes on the ITO electrode, which is remotely connected to the gate of the FET. The FET measures the surface potential of the ITO, providing the final detection signal.

Incubation is a critical step in enhancing signal resolution. Our signal is based on the filtration of HRP-AuNP, specifically detecting unbound HRP-AuNP in the detection zone. With incubation, more HRP-AuNP binds to E2 antibodies in the testing solution during step 2 of Figure 5A. Consequently, more HRP-AuNP is retained in the detection zone, and less HRP-AuNP reaches the signal zone, leading to a lower signal in Figure S14A. Without incubation, there is insufficient time for the formation of E2 antibody-HRP-AuNP complexes in the testing solution. As a result, HRP-AuNP flows nonspecifically into the signal zone, producing a higher signal. Due to this effect, there was an insignificant signal difference between samples containing 184 and 576 pg/mL of E2 (Figure S14A). The signal resolution, determined by the difference in REEA signal between plasma samples containing 184 and 576 pg/mL of E2, saturated after 15 min of incuba-

tion. This was optimized as the ideal incubation time for the procedure (Figure S14B).

Another critical parameter in the REEA system is the concentration of AuNP-HRP-E2 conjugates. When the concentration is too high, the binding sites of E2 antibodies during incubation become fully occupied, regardless of the free E2 concentration in the testing solution. To determine the optimal concentration of AuNP-HRP-E2 conjugates, the same paper fluidics setup was used with two testing solutions: one containing 5 ng/mL of free E2 and the other without free E2. The signal-to-noise ratio (SNR) was calculated by dividing the signal from the 5 ng/mL E2 sample by the signal from the sample with no E2, as a function of the AuNP-HRP-E2 conjugate concentration. An SNR of 1 indicates no signal differentiation between the two scenarios. Reducing the AuNP-HRP-E2 concentration corresponding to 0.1 OD₅₂₅ increased the SNR to 5, which was identified as the optimal concentration for the competitive immunoassay (Figure 5B).

Measurement time was optimized to balance signal resolution with detection speed, constrained by the enzymatic reaction duration. The current cartridge design, comprising detection, bridge, and signal generation zones, required 600 s to achieve precise signals at concentrations below 5 pg/mL (Figure S15). Notably, the maximum REEA signal was reached within 150–200 s (Figure S15), with approximately half of the total

measurement time attributed to fluid flow through the detection and signal zones.

Under the optimized testing conditions, the E2-spiked sample was evaluated across a concentration range of 328 fg/mL to 1 ng/mL to determine the LOD of the system (Figure 5C). The LOD was calculated to be approximately 146 fg/mL using the 3σ rule, with the CV for each E2 concentration being less than 9.2%. Additionally, clinical plasma samples with E2 concentrations ranging from 19 to 4,551 pg/mL were tested (Figure 5D), showing an r^2 of 0.963 and a standard error of the estimate ($S_{y/x}$) of 0.15, as determined by logarithmic regression analysis when compared with results from FDA-cleared clinical immunoassay (Figure 5D).

Conclusions and outlook

Conventional LFAs are used as standard POC tools due to their simplicity, robustness, and cost-effectiveness. Their dry reagent format enhances stability, with optimized components demonstrating a shelf life of up to 2 years.³⁸ While most LFAs rely on optical signals or visual inspection, they often fall short of the required LOD for a broad range of biomarkers. A key advantage of the REEA platform is its ability to integrate LFAs with FET biosensors for electrical quantification. This integration provides several benefits: (1) it simplifies the surface modification of FET biosensors by utilizing dry chemistry within the LFA system and (2) the REEA platform, along with the simple fluidics of LFAs, eliminates the need for complex capture-release methods typically required for FETs. These conventional methods involve extensive washing steps and buffer dilutions to overcome Debye length challenges and matrix effects, which the REEA platform bypasses.

Further development will focus on enhancing usability by enabling the direct application of finger-prick whole-blood samples. This will involve integrating a plasma separation capability into the paper fluidics to facilitate plasma release into the assay cartridge. Pre-drying components such as AuNP-HRP-E2, stabilizers, and surfactants within the paper fluidic system will streamline the workflow, while optimizing paper fluidic structures and antibody screening could eliminate the need for incubation, ensuring signal differentiation with minimal user intervention.

The current detection time of 10 min, required for high signal resolution, can be reduced, as the maximum REEA signal is generated in approximately 200 s (Figure S15). The lateral paper strip design accounts for approximately 50% of the measurement time, primarily due to fluid passage. A vertical paper fluidics structure could reduce wetting time while maintaining the capture efficiency.³⁹

While our study demonstrates the feasibility of the REEA platform as a diagnostic tool, we recognize that several challenges remain in translating this platform from laboratory research to practical clinical applications. Large-scale manufacturing processes, quality control standards, and cost-efficiency assessments will be essential to establishing a viable alternative to conventional laboratory testing. Assuming current material costs in scaled-up production, the estimated cost of goods sold is projected to range between \$1 and \$2. Additionally, user variability and environmental factors such as temperature and humidity could affect performance in home settings, highlighting the

need for robustness testing under diverse real-world conditions. Evaluating long-term stability of the device and reagents, particularly under varied storage environments, will also be critical to ensure reliable performance over an extended shelf life. Future work will prioritize addressing these challenges to facilitate the transition of the REEA platform from proof-of-concept to a validated, commercially viable diagnostic system.

Although primarily optimized for E2 detection, the REEA platform exhibits potential for adaptation to a broader range of biomarkers for metabolic panels such as luteinizing hormone, progesterone, thyroid-stimulating hormone, and cortisol and for chronic conditions such as troponin-9 and tau proteins associated with Alzheimer's disease, enhancing its versatility in personalized medicine and diagnostics. In line with the global shift toward home-based healthcare, our platform addresses the critical need for accurate, cost-effective, and rapid diagnostics beyond traditional clinical settings. This development represents a significant step toward improving healthcare accessibility, supporting efforts to meet the growing demands on healthcare systems worldwide.

METHODS

Chemicals and other resources

The following chemicals were purchased for the study: TMYP (Sigma-Aldrich, AMBH303C58D3), TMLP (Sigma-Aldrich, T790 06-25G), MP (Sigma-Aldrich, M18655), FP (Sigma-Aldrich, F13207), IP (Sigma-Aldrich, I10201), CP (ThermoFisher Scientific, 181001000), BP (Sigma-Aldrich, B75808), TCP (Sigma-Aldrich, T55301), AD (Sigma-Aldrich, A88255), T (Sigma-Aldrich, 236 314), FA (Sigma-Aldrich, F3800), OPD (Sigma-Aldrich, P23938), TMYA (Sigma-Aldrich, AMBH303C5E71), and CA (Sigma-Aldrich, C22415). Additionally, anti- 17β -estradiol monoclonal antibody (CD Creative Diagnostics, DMATBT-49063MH), E2-HRP conjugate (CD Creative Diagnostics, DAGA-025B-HRP), and 17β -estradiol standard (CD Creative Diagnostics, DAGS 030) were acquired. TMB (Sigma-Aldrich, 87750), CC (Sigma-Aldrich, C7527-100G), HRP (Toyobo, PEO-301), and ChOx (Toyobo, CHO-301) were also obtained. ITO on a polyethylene terephthalate (ITO/PET) (Sigma-Aldrich, 639303) was used as the sensing electrode. Gold nanoparticles (Ted Pella, 15704-1), acetonitrile (Sigma-Aldrich, 34851), 10% BSA block (Thermo Scientific, 37525), mouse IgG-HRP (SouthernBiotech, 0107-05), goat anti-mouse IgG (SouthernBiotech, 1033-01), goat anti-mouse IgG-HRP (SouthernBiotech, 1033-05), H_2O_2 solution (Sigma-Aldrich, 88597), and estradiol (Sigma-Aldrich, E1024) were purchased for the study.

Solution test

ITO/PET was cut into $1 \times 2 \text{ cm}^2$ pieces and cleaned with isopropanol for 20 min before use in the standard RGFET setup in Figure 2 with an Ag/AgCl reference electrode. There are several compelling reasons for employing ITO/PET: firstly, ITO is commercially available, providing reliable pH sensitivity on plastic substrates, which is essential for scalable production. Additionally, the flexibility of the ITO/PET combination allows for easy customization of electrode shapes using laser cutting technology, offering both precision and adaptability in design.

Furthermore, ITO layers provide robustness while maintaining the flexibility needed for cartridge assembly.

For the solution-based tests, the optimal FP concentration for the REEA was determined to be 10 mM, as higher concentrations resulted in signal saturation (Figure S16). Therefore, a concentration of 10 mM was used in all subsequent experiments to ensure consistency and accuracy in the REEA process during solution testing.

For Figure 2, 1 M of each phenolic substrate was initially diluted in acetonitrile. Each substrate solution and H₂O₂ were further diluted in 1× PBS to final concentrations of 30 and 15 mM, respectively. HRP was also diluted to 3 µg/mL in 1× PBS. Sequentially, 10 µL of each solution was added to the ITO electrode in the following order: HRP solution, substrate solution, and H₂O₂ solution, resulting in final concentrations of 10 mM for the substrate, 5 mM for H₂O₂, and 1 µg/mL for HRP, with a total testing volume of 30 µL. For Figure 2E, different concentrations of HRP, ranging from 1 pg/mL to 100 µg/mL, were prepared in 1× PBS and human plasma (purchased from Kalen Biomedical). An Ag/AgCl reference electrode was immersed in the solution during measurements. Each ITO electrode was discarded after a single measurement, and the standard Ag/AgCl reference electrode was washed in 70% ethanol for 5 min, followed by rinsing with DI water three times before being used in the next experiment.

For the solution-based tests using the ITO-Cu electrode in Figure S9, the ITO electrode was laser-cut into a spoon shape using an OMTech laser cutter. The cutting was performed at a speed of 50 mm/s with a current of 0.25 A. The circular part of the spoon-shaped electrode had a diameter of 6 mm, and a 2 × 2 mm notch was cut to accommodate a rectangular Cu electrode (2 × 20 mm), which was inserted into the notch.

For the solution tests, 10 µL of HRP solution, diluted in 1× PBS to different concentrations, was first placed on the electrode. Subsequently, 10 µL of 30 mM FP solution (diluted in acetonitrile) and 10 µL of 15 mM H₂O₂ solution were sequentially added, resulting in final concentrations of 5 mM H₂O₂ and 10 mM FP in the test solution. Each ITO-Cu electrode was discarded after a single measurement.

Cartridge fabrication

Following the cleaning process, ITO (1 × 3 cm²) and Cu (1 × 3 cm²) electrodes were laser-cut to the desired dimensions using an OMTech laser cutter at a speed of 50 mm/s and a current of 0.25 A. Paper fluidic strips were constructed using NC membrane (MilliporeSigma, HF13502XSS) mounted on laminated cards (MilliporeSigma, HF000MC100) with release liners. The NC strip in the signal zone was spotted with 10 µL of 10 mg/mL ChOx diluted in 1× PBS, which was determined to be the optimal concentration in Figure 3D. The detection zone was spotted with 5 µL of 200 µg/mL goat anti-mouse IgG in 0.2% BSA solution to ensure sufficient antibody concentration for capturing 1.5 µg/mL E2 antibody in the running buffer. NC strips were dried for 15 min at 37°C and stored with silica gel. Each NC strip was affixed to the designated areas of the cartridge's acrylic frame. A cotton linter pad (CF7, Cytiva), sliced into 0.4 × 0.6 cm, was placed between the detection and signal zones using an acrylic jig supported by a clip. The ITO was mounted over the ChOx-functionalized NC strip in the signal zone using a magnet.

Assay operation

For colorimetry tests in Figure 3A, the NC strip functionalized with 2.5 µL of anti-17β-estradiol monoclonal antibody diluted in 0.1% BSA was affixed onto the cartridge acryl flame and loaded with 100 µL of 1 µg/mL anti-mouse IgG-HRP in 2% BSA in PBS solution for 5 min. Then, 200 µL of 2% BSA washing buffer was injected for 3 min through the main chamber of the cartridge, followed by 100 µL of 20% TMB solution. New NC strips from the same batch underwent the same washing step and were characterized by injecting 100 µL of 5 mM FP and 5 mM H₂O₂ solutions.

All NC strips used in Figures 3C–3F were functionalized with 10 µL of 10 mg/mL ChOx diluted in 1× PBS. AuNPs (15 nm) were used for E2-HRP conjugation. AuNP-HRP-E2 conjugates were synthesized by adding 1 mL of AuNP solution (1 OD), 100 µL of 0.1 M borate buffer (pH 8.5), and 10 µL of 1 mg/mL E2-HRP into a sterile Eppendorf tube. The mixture was incubated for 45 min at room temperature, followed by the addition of 100 µL of 1% BSA in PBS to act as a blocking agent, preventing nonspecific binding. After a 30-min incubation, the AuNP conjugates were centrifuged at 4°C for 15 min at 15,000 rpm, washed three times with 1 mL of 10 mM Tris buffer (pH 7.4), and resuspended in 100 µL of storage buffer (0.1 M borate buffer [pH 8.5], with 0.1% BSA and 1% sucrose). The final concentration of AuNP-E2-HRP conjugates was confirmed by OD measurement at 525 nm using a Biotek PowerWave XS Microplate Reader.

For testing solutions used in Figure 3C, 1M substrates were diluted in acetonitrile, then further diluted in 2% BSA to achieve a final concentration of 5 mM, which is the optimized concentration as shown in Figure 3F. Similarly, 1 M CC was diluted in deionized water and then in 2% BSA to a final concentration of 25 mM, which is the optimized concentration shown in Figure 3E. AuNPs were added to the testing solution, resulting in a final concentration of 0.05 OD. A total of 200 µL of the testing solution, containing different substrates at the same concentration (5 mM), was injected into the NC strips for Figure 3C through main chamber of the cartridge flame. For Figure 3D, NC strips with dried ChOx concentrations ranging from 0 to 11 mg/mL were prepared. A total of 200 µL of testing solution, containing 0.05 OD AuNP-HRP-E2 conjugate, 25 mM CC, and 5 mM FP, was used, with 2% BSA in 1× PBS as the base buffer.

In Figures 3E and 3F, A total of 200 µL testing solution for Figure 3E included varying concentrations of CC, ranging from 0.048 to 100 mM, while maintaining 0.05 OD AuNP-HRP-E2 conjugate and 5 mM FP with 2% BSA in 1× PBS as the base buffer. For Figures 3F and 3A total of 200 µL testing solution contained varying concentrations of FP, ranging from 0.015 to 10 mM, while maintaining 0.05 OD AuNP-HRP-E2 conjugate and 25 mM CC with 2% BSA in 1× PBS as the base buffer.

The optimized running buffer through experiments in Figures 4A and 4B contained 2% BSA, 0.2% IGEPAL, and 2.5% PVP (detailed in Table S3). The running buffer including 2% BSA, 0.2% IGEPAL, and 2.5% PVP is further mixed with either E2-spiked or clinical plasma samples for experiments in Figures 5B–5D. A stock solution of 17β-estradiol standard at a concentration of 0.5 mg/mL was prepared by dissolving the compound in isopropanol. For E2-spiked sample measurements, a 100-fold specific concentration of the E2 solution was prepared through serial dilution with

isopropanol and spiked into the running buffer at a final concentration of 3% (v/v). For clinical plasma sample measurements, 5 μ L of the plasma sample was mixed with 95 μ L of running buffer, resulting in a final dilution factor of 60 \times for operation. In both cases, 100 μ L of the prepared sample solution was mixed with 100 μ L of antibody solution (1.5 μ g/mL E2 antibody in running buffer) and incubated for 15 min after vortex mixing. Then, 100 μ L of substrate solution (75 mM CC, 15 mM FP in running buffer) was added, and 300 μ L of this final mixture was injected into the injection zone. Measurements were taken for 10 min using a handheld reader.

Measurement system

All experiments for [Figure 2](#) were conducted using a semiconductor analyzer with an Ag/AgCl reference electrode system. The ITO electrode of the cartridge was connected to the gate of a commercial n-type metal-oxide-semiconductor field-effect transistor (MOSFET) (CD4007UB) using an alligator clip. To ensure consistency, the same MOSFET was used throughout the experiment. The Ag/AgCl reference electrode was in contact with the solution via injections into the main chamber. Transfer curves were obtained using a Keithley 4200A semiconductor analyzer, with a source-drain voltage set at 50 mV, and a gate voltage sweep ranging from 0 to 3 V in double-sweep mode. Transfer curves were measured repeatedly for 5 min under each plasma sample, and V_{th} was calculated as the gate voltage corresponding to a drain current of 1 μ A in each transfer curve. For [Figures 3](#) and [5](#), all experiments were conducted using a handheld FET reader device and a copper reference electrode. The gate and drain voltages were fixed at 2 and 3 V, respectively, with power supplied via a USB Type-C connection to a laptop. V_{out} was measured every second, and the signal was monitored in real-time through software (Arduino IDE) installed on the laptop. All CV values were calculated as the standard deviation divided by the mean. All error bars represent the standard error, calculated as the standard deviation divided by the square root of the sample size.

Clinical sample test: De-identified

Lithium heparin plasma from leftover patient samples collected at The University of Chicago Medical Center with E2 concentrations ranging from 19 to 4,551 pg/mL were stored at -80°C until use. Samples were collected under a quality assurance protocol, which qualified for an institutional review board waiver and no patient identifiers were collected. E2 concentrations were quantified using the Cobas e801 analyzer (Roche Diagnostics). After thawing, the samples were stored at 2°C–8°C for up to 7 days.

RESOURCE AVAILABILITY

Lead contact

Further information and requests for resources should be directed to the lead contact, Junhong Chen (junhongchen@uchicago.edu).

Materials availability

This study did not generate new unique reagents.

Data and code availability

All data of this study are available within the article and [supplemental information](#).

ACKNOWLEDGMENTS

This work was financially supported by a University of Chicago Faculty Start-up fund and by a Walder Foundation grant 22-01071.

AUTHOR CONTRIBUTIONS

Electrical measurements and device fabrication were carried out by H.-J.J. and X.S. Interpretation of data and design of platform were carried out by H.-J.J., H.-A.J., X.S., E.T., J.W., J.H., and J.H.C. Simulation was carried out by R.D. The reader device was designed by B.R. and W.Z. The manuscript was prepared by H.-J.J., H.-A.J., J.W., and J.H.C. Plasma samples were retrieved and evaluated by G.C. and K.-T.J.Y. All authors edited the manuscript and commented on it. The project was supervised by J.H.C.

DECLARATION OF INTERESTS

The authors have a pending patent application related to the technology presented in this study. H.-J.J. and H.-A.J., co-founders of Kompass Diagnostics Inc., have a commercial interest in the diagnostic technology described in this work.

DECLARATION OF GENERATIVE AI AND AI-ASSISTED TECHNOLOGIES IN THE WRITING PROCESS

During the preparation of this work, the authors used ChatGPT 4 to proofread the text, ensure readability, reducing duplicate statements, and help provide succinct summaries. The tool was not used to generate any information besides editing and summaries. After using this tool, the authors reviewed and edited the content as needed and take full responsibility for the content of the published article.

SUPPLEMENTAL INFORMATION

Supplemental information can be found online at <https://doi.org/10.1016/j.device.2025.100807>.

Received: January 22, 2025

Revised: April 24, 2025

Accepted: April 28, 2025

Published: May 23, 2025

REFERENCES

- Yakoub, Y., Ashton, N.J., Strikwerda-Brown, C., Montoliu-Gaya, L., Kari-Kari, T.K., Kac, P.R., Gonzalez-Ortiz, F., Gallego-Rudolf, J., Meyer, P.F., St-Onge, F., et al. (2023). Longitudinal blood biomarker trajectories in pre-clinical Alzheimer's disease. *Alzheimer's Dement.* 19, 5620–5631. <https://doi.org/10.1002/alz.13318>.
- Kimenai, D.M., Anand, A., de Bakker, M., Shipley, M., Fujisawa, T., Lyngbakken, M.N., Hveem, K., Omland, T., Valencia-Hernández, C.A., Lindbohm, J.V., et al. (2023). Trajectories of cardiac troponin in the decades before cardiovascular death: a longitudinal cohort study. *BMC Med.* 21, 216. <https://doi.org/10.1186/s12916-023-02921-8>.
- Bourion-Bedes, S., Tarquinio, C., Batt, M., Tarquinio, P., Lebreuilly, R., Sorsana, C., Legrand, K., Rousseau, H., and Baumann, C. (2021). Psychological impact of the COVID-19 outbreak on students in a French region severely affected by the disease: results of the PIMS-CoV 19 study. *Psychiatry Res.* 295, 113559. <https://doi.org/10.1016/j.psychres.2020.113559>.
- Brezina, P.R., Haberl, E., and Wallach, E. (2011). At home testing: optimizing management for the infertility physician. *Fertil. Steril.* 95, 1867–1878. <https://doi.org/10.1016/j.fertnstert.2011.01.001>.
- Wu, A.K., Odisho, A.Y., Washington, S.L., Katz, P.P., and Smith, J.F. (2014). Out-of-Pocket Fertility Patient Expense: Data from a Multicenter Prospective Infertility Cohort. *J. Urol.* 191, 427–432. <https://doi.org/10.1016/j.juro.2013.08.083>.

6. Cánovas, R., Daems, E., Langley, A.R., and De Wael, K. (2023). Are aptamer-based biosensing approaches a good choice for female fertility monitoring? A comprehensive review. *Biosens. Bioelectron.* 220, 114881. <https://doi.org/10.1016/j.bios.2022.114881>.
7. Harris, J.A., Menke, M.N., Haefner, J.K., Moniz, M.H., and Perumalswami, C.R. (2017). Geographic access to assisted reproductive technology health care in the United States: a population-based cross-sectional study. *Fertil. Steril.* 107, 1023–1027. <https://doi.org/10.1016/j.fertnstert.2017.02.101>.
8. Wu, A.K., Elliott, P., Katz, P.P., and Smith, J.F. (2013). Time costs of fertility care: the hidden hardship of building a family. *Fertil. Steril.* 99, 2025–2030. <https://doi.org/10.1016/j.fertnstert.2013.01.145>.
9. Adeleye, A.J., Kawwass, J.F., Brauer, A., Storment, J., Patrizio, P., and Feinberg, E. (2023). The mismatch in supply and demand: reproductive endocrinology and infertility workforce challenges and controversies. *Fertil. Steril.* 120, 403–405. <https://doi.org/10.1016/j.fertnstert.2023.01.007>.
10. Cauley, J.A., Lucas, F.L., Kuller, L.H., Stone, K., Browner, W., and Cummings, S.R. (1999). Elevated serum estradiol and testosterone concentrations are associated with a high risk for breast cancer. Study of Osteoporotic Fractures Research Group. *Ann. Intern. Med.* 130, 270–277. https://doi.org/10.7326/0003-4819-130-4_part_1-199902160-00004.
11. Ankarberg-Lindgren, C., and Norjavaara, E. (2009). Estradiol in pediatric endocrinology. *Am. J. Clin. Pathol.* 132, 978–980. <https://doi.org/10.1309/AJCPA65OUUFA5OAN>.
12. Meczekalski, B., Podfigurna-Stopa, A., and Genazzani, A.R. (2010). Hypoestrogenism in young women and its influence on bone mass density. *Gynecol. Endocrinol.* 26, 652–657. <https://doi.org/10.3109/09513590.2010.486452>.
13. O'Donnell, E., Harvey, P.J., Goodman, J.M., and De Souza, M.J. (2007). Long-term estrogen deficiency lowers regional blood flow, resting systolic blood pressure, and heart rate in exercising premenopausal women. *Am. J. Physiol. Endocrinol. Metab.* 292, E1401–E1409. <https://doi.org/10.1152/ajpendo.00547.2006>.
14. Conde, D.M., Verdaide, R.C., Valadares, A.L.R., Mella, L.F.B., Pedro, A.O., and Costa-Paiva, L. (2021). Menopause and cognitive impairment: A narrative review of current knowledge. *World J. Psychiatr.* 11, 412–428. <https://doi.org/10.5498/wjp.v11.i8.412>.
15. Szeliga, A., Calik-Ksepka, A., Maciejewska-Jeske, M., Grymowicz, M., Smolarczyk, K., Kostrzak, A., Smolarczyk, R., Rudnicka, E., and Meczekalski, B. (2021). Autoimmune Diseases in Patients with Premature Ovarian Insufficiency-Our Current State of Knowledge. *Int. J. Mol. Sci.* 22, 2594. <https://doi.org/10.3390/ijms22052594>.
16. Li, J., Li, L., Bian, Y., Yu, Y., Qiang, Z., Zhang, Y., and Li, H. (2020). Quantitation of estradiol by competitive light-initiated chemiluminescent assay using estriol as competitive antigen. *J. Clin. Lab. Anal.* 34, e23014. 1002/jcla.23014.
17. Rosner, W., Hankinson, S.E., Sluss, P.M., Vesper, H.W., and Wierman, M. E. (2013). Challenges to the Measurement of Estradiol: An Endocrine Society Position Statement. *J. Clin. Endocrinol. Metab.* 98, 1376–1387. <https://doi.org/10.1210/jc.2012-3780>.
18. Lopredise, A., Calabretta, M.M., Montali, L., Zangheri, M., Guardigli, M., Mirasoli, M., and Michelini, E. (2021). Bioluminescence goes portable: recent advances in whole-cell and cell-free bioluminescence biosensors. *Luminescence* 36, 278–293. <https://doi.org/10.1002/bio.3948>.
19. Yao, X., Wang, Z., Zhao, M., Liu, S., Su, L., Dou, L., Li, T., Wang, J., and Zhang, D. (2021). Graphite-like carbon nitride-laden gold nanoparticles as signal amplification label for highly sensitive lateral flow immunoassay of 17beta-estradiol. *Food Chem.* 347, 129001. <https://doi.org/10.1016/j.foodchem.2021.129001>.
20. Na, W., Park, J.W., An, J.H., and Jang, J. (2016). Size-controllable ultrathin carboxylated polypyrrole nanotube transducer for extremely sensitive 17beta-estradiol FET-type biosensors. *J. Mater. Chem. B* 4, 5025–5034. <https://doi.org/10.1039/c6tb00897f>.
21. Jang, H.J., Zhuang, W., Sui, X., Ryu, B., Huang, X., Chen, M., Cai, X., Pu, H., Beavis, K., Huang, J., and Chen, J. (2023). Rapid, Sensitive, Label-Free Electrical Detection of SARS-CoV-2 in Nasal Swab Samples. *ACS Appl. Mater. Interfaces* 15, 15195–15202. <https://doi.org/10.1021/acsami.3c00331>.
22. Xu, S., Wang, T., Liu, G., Cao, Z., Frank, L.A., Jiang, S., Zhang, C., Li, Z., Krasitskaya, V.V., Li, Q., et al. (2021). Analysis of interactions between proteins and small-molecule drugs by a biosensor based on a graphene field-effect transistor. *Sensor Actuat. B-Chem.* 326, 128991. <https://doi.org/10.1016/j.snb.2020.128991>.
23. Tian, M., Wei, J., Lv, E., Li, C., Liu, G., Sun, Y., Yang, W., Wang, Q., Shen, C., Zhang, C., et al. (2024). Drug evaluation platform based on non-destructive and real-time *in situ* organoid fate state monitoring by graphene field-effect transistor. *Chem. Eng. J.* 498, 155355.
24. Jang, H.J., Sui, X., Zhuang, W., Huang, X., Chen, M., Cai, X., Wang, Y., Ryu, B., Pu, H., Ankenbruck, N., et al. (2022). Remote Floating-Gate Field-Effect Transistor with 2-Dimensional Reduced Graphene Oxide Sensing Layer for Reliable Detection of SARS-CoV-2 Spike Proteins. *ACS Appl. Mater. Interfaces* 14, 24187–24196. <https://doi.org/10.1021/acsami.2c04969>.
25. Jang, H.J., Joung, H.A., Goncharov, A., Kanegusuku, A.G., Chan, C.W., Yeo, K.T.J., Zhuang, W., Ozcan, A., and Chen, J. (2024). Deep Learning-Based Kinetic Analysis in Paper-Based Analytical Cartridges Integrated with Field-Effect Transistors. *ACS Nano* 18, 24792–24802. <https://doi.org/10.1021/acs.nano.4c02897>.
26. Veitch, N.C. (2004). Horseradish peroxidase: a modern view of a classic enzyme. *Phytochemistry* 65, 249–259. <https://doi.org/10.1016/j.phytochem.2003.10.022>.
27. Sajid, M., Kawde, A.N., and Daud, M. (2015). Designs, formats and applications of lateral flow assay: A literature review. *J. Saudi Chem. Soc.* 19, 689–705.
28. Pirzad, R., Newman, J.D., Dowman, A.A., and Cowell, D.C. (1994). Horseradish-Peroxidase Assay - Radical Inactivation or Substrate-Inhibition - Revision of the Catalytic Sequence Following Mass-Spectral Evidence. *Analyst* 119, 213–218. <https://doi.org/10.1039/an9941900213>.
29. Sturgeon, B.E., Battenburg, B.J., Lyon, B.J., and Franzen, S. (2011). Revisiting the Peroxidase Oxidation of 2,4,6-Trihalophenols: ESR Detection of Radical Intermediates. *Chem. Res. Toxicol.* 24, 1862–1868. <https://doi.org/10.1021/tx200215r>.
30. Gazaryan, I.G., Chubar, T.A., Ignatenko, O.V., Mareeva, E.A., Orlova, M.A., Kapeliuch, Y.L., Savitsky, P.A., Rojkova, A.M., and Tishkov, V.I. (1999). Tryptophanless recombinant horseradish peroxidase: Stability and catalytic properties. *Biochem. Biophys. Res. Co.* 262, 297–301. <https://doi.org/10.1006/bbrc.1999.1155>.
31. Jang, H.J., Lee, T., Song, J., Russell, L., Li, H., Dailey, J., Searson, P.C., and Katz, H.E. (2018). Electronic Cortisol Detection Using an Antibody-Embedded Polymer Coupled to a Field-Effect Transistor. *ACS Appl. Mater. Interfaces* 10, 16233–16237. <https://doi.org/10.1021/acsami.7b18855>.
32. Jang, H.J., Wagner, J., Li, H., Zhang, Q., Mukhopadhyaya, T., and Katz, H.E. (2019). Analytical Platform To Characterize Dopant Solution Concentrations, Charge Carrier Densities in Films and Interfaces, and Physical Diffusion in Polymers Utilizing Remote Field-Effect Transistors. *J. Am. Chem. Soc.* 141, 4861–4869. <https://doi.org/10.1021/jacs.8b13026>.
33. Pirzad, R., Newman, J.D., Dowman, A.A., and Cowell, D.C. (1989). Horseradish-Peroxidase Assay - Optimization of Carbon-Fluoride Bond Breakage and Characterization of Its Kinetics Using the Fluoride Ion-Selective Electrode. *Analyst* 114, 1583–1586. <https://doi.org/10.1039/an9891401583>.
34. Osman, A.M., Boeren, S., Boersma, M.G., Veeger, C., and Rietjens, I.M. (1997). Microperoxidase/H₂O₂-mediated alkoxylating dehalogenation of halophenol derivatives in alcoholic media. *Proc. Natl. Acad. Sci. USA* 94, 4295–4299. <https://doi.org/10.1073/pnas.94.9.4295>.
35. Thapa, B., and Schlegel, H.B. (2017). Improved pK(a) Prediction of Substituted Alcohols, Phenols, and Hydroperoxides in Aqueous Medium Using Density Functional Theory and a Cluster-Continuum Solvation

- Model. *J. Phys. Chem. A* 121, 4698–4706. <https://doi.org/10.1021/acs.jpca.7b03907>.
36. Jang, H.J., Ahn, J., Kim, M.G., Shin, Y.B., Jeun, M., Cho, W.J., and Lee, K. H. (2015). Electrical signaling of enzyme-linked immunosorbent assays with an ion-sensitive field-effect transistor. *Biosens. Bioelectron.* 64, 318–323. <https://doi.org/10.1016/j.bios.2014.09.020>.
37. Huang, Q., Huang, Q., Pinto, R.A., Griebenow, K., Schweitzer-Stenner, R., and Weber, W.J., Jr. (2005). Inactivation of horseradish peroxidase by phenoxyl radical attack. *J. Am. Chem. Soc.* 127, 1431–1437. <https://doi.org/10.1021/ja045986h>.
38. O'Farrell, B. (2009). Evolution in Lateral Flow-Based Immunoassay Systems. *Lateral Flow Immunoassay*, 1–33. https://doi.org/10.1007/978-1-59745-240-3_1.
39. Ballard, Z.S., Joung, H.A., Goncharov, A., Liang, J., Nugroho, K., Di Carlo, D., Garner, O.B., and Ozcan, A. (2020). Deep learning-enabled point-of-care sensing using multiplexed paper-based sensors. *npj Digit. Med.* 3, 66. <https://doi.org/10.1038/s41746-020-0274-y>.

Supplemental information

**Radical-mediated electrical enzyme assay
for estradiol: Toward point-of-care diagnostics**

Hyun-June Jang (현준장), Hyou-Arm Joung (효암정), Xiaoao Shi, Rui Ding, Justine Wagner, Erting Tang, Wen Zhuang, Byunghoon Ryu (병훈류), Guanmin Chen, Kiang-Teck Jerry Yeo, Jun Huang, and Junhong Chen

Table of Contents

Table S1. Material costs of cartridge components per test

Figure S1. Electrical properties of the FET

Figure S2. Cartridge structure

Figure S3. pH sensitivity of the RGFET

Figure S4. Screening of substrates for REEA signal

Table S2. Density functional theory simulations for REEA

Figure S5. REEA signal depending on HRP concentration

Figure S6. pH sensitivity of the RGFET at a handheld device

Figure S7. Interference tests from different paper materials

Figure S8. Performance comparison of RGFET, measured by a semiconductor analyzer and at a handheld device

Figure S9. Reference electrode tests in REEA signal

Figure S10. REEA signal of AuNP-HRP-E2 conjugate tested in solution phase

Figure S11. REEA signal tested on paper material

Figure S12. Titration curves of the REEA signal depending on the concentration of AuNP-HRP-E2 conjugate in paper material

Figure S13. Optimization of REEA components

Table S3. Optimization of running buffer components

Figure S14. Incubation effect

Figure S15. Signal resolution depending on measurement time

Figure S16. Optimization of FP concentration for REEA.

Table S1. Breaking down of material cost of cartridge components per test.

	Items	cost/test (¢)
Materials	NC membrane	4.9
	Absorbent pad	3.8
	Electrodes	2.8
	Acrylic case	4.4
Material total		16.1
Reagents	anti-E2 antibody	21.8
	Estradiol-HRP	3.7
	anti-mouse IgG	2.4
	BSA	3.0
	Choline Oxidase	2.0
	Glod nanoparticles	2.3
<u>Others (chemical, buffer, ect)</u>		4.3
Reagent total		39.6
Total cost per test		55.6

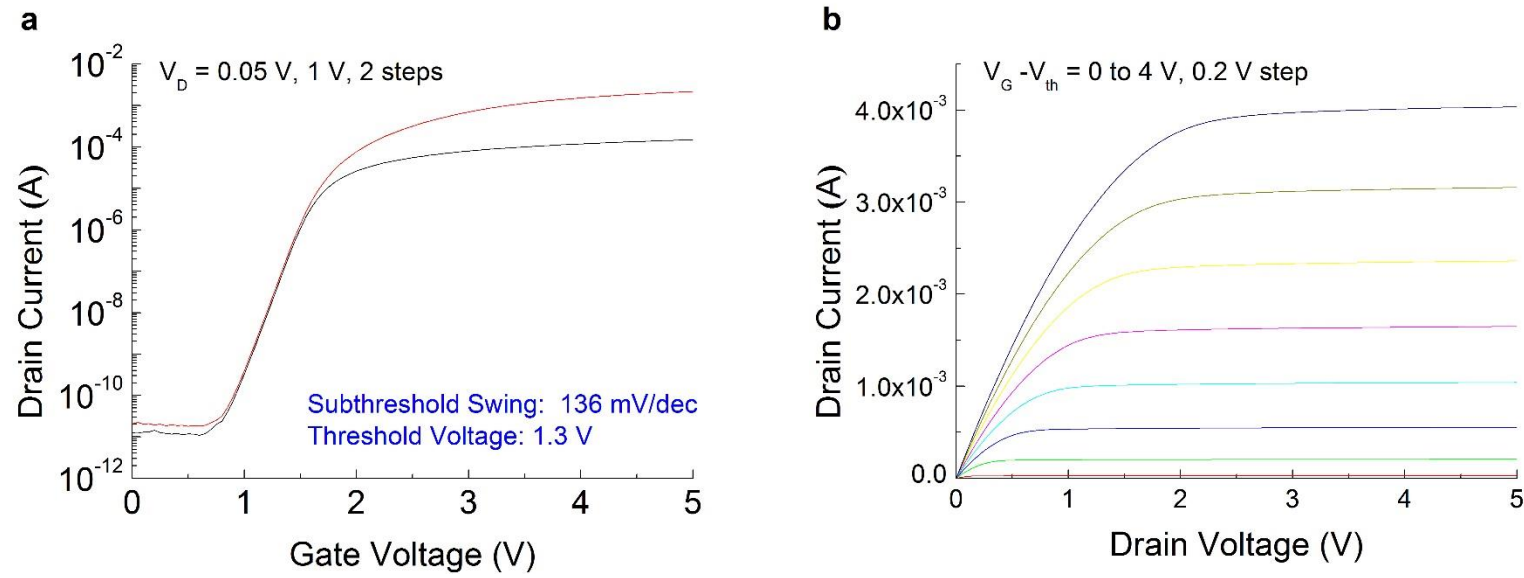


Figure S1. Electrical properties of the FET. (a) Representative transfer curves and (b) output characteristic of commercial FET, CD4007UB.

Subthreshold swing of 136 mV/dec and threshold voltage of 1.3 V were observed in the commercial FET.

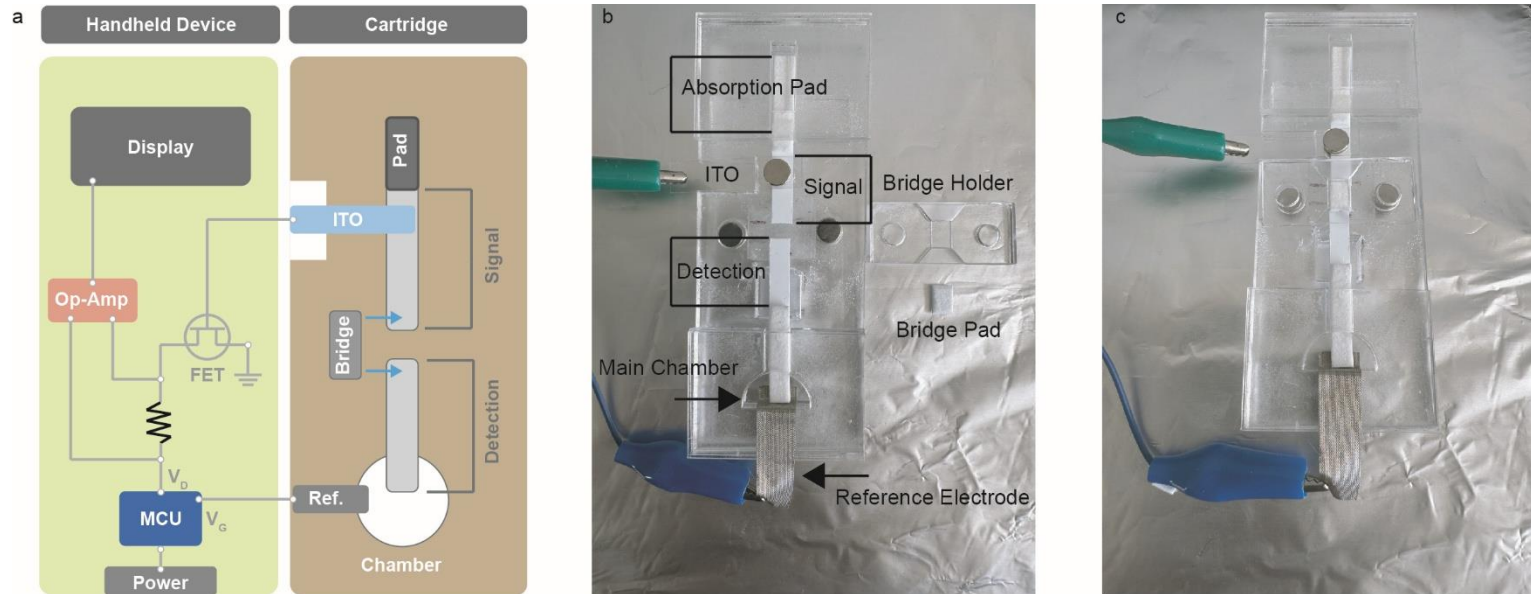


Figure S2. The cartridge structure. (a) Schematics of essential components of the handheld device and its connection with the cartridge. The handheld device is compact, with dimensions of approximately 2.5 cm by 4 cm and features a display screen for real-time readouts. The paper fluidics cartridge is designed to facilitate sample movement and reaction processes. A reference electrode, a copper electrode, is used to apply gate voltage (V_G) for the FET from the microcontroller unit (MCU) integrated into the handheld device. The drain voltage (V_D) is independently supplied to the drain terminal by the MCU. The ITO working electrode built in the paper fluidics cartridge is remotely connected to the gate of the FET built into the handheld device. Once the testing sample is injected into the main chamber, the electrical connection between the working and reference electrodes is established. The output voltage in our handheld device system is primarily derived from the voltage drop across the resistance at the drain terminal, measured through differential voltage amplification using an operational amplifier (op-amp). The output voltage is closely related to the drain current, essentially representing the drain current multiplied by a constant resistance. In other words, a shift in the threshold voltage results in a change in the drain current observed in the transfer curves of FET, which, in turn, results in a corresponding change in the output voltage of the handheld device. Actual photos of (b) the cartridge components and (c) the fully assembled cartridge.

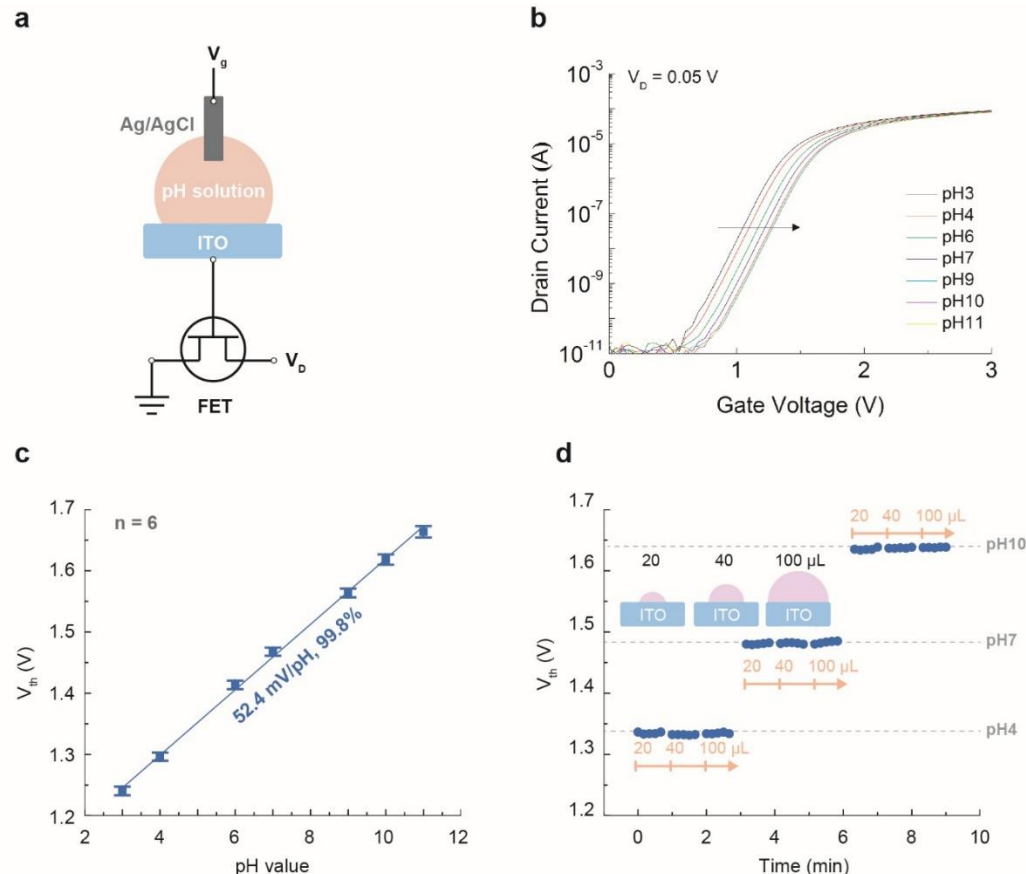


Figure S3. pH sensitivity of the RGFET. (a) Schematic of the RGFET setup, where the ITO electrode is remotely connected to the gate of a commercial FET. A pH solution is placed on top of the ITO, with a standard Ag/AgCl reference electrode immersed in the solution. The gate voltage (V_g) is supplied from a semiconductor analyzer through the Ag/AgCl reference electrode. Drain voltage (V_D) is set at 50 mV. (b) Shifts in transfer curves on ITO under varying pH conditions, ranging from pH 3 to 11. The curves exhibit parallel shifts without changes in shape, indicating that pH-dependent variations in the surface potential of ITO are responsible for the shifts. . (c) pH sensitivity of the ITO, calculated from threshold voltage shifts under varying pH conditions, estimated to be 52.4 mV/pH with 99.8% linearity across the pH range of 3 to 11. (d) The V_{th} response to pH, showing independence from volume differences of the pH solution on the ITO.

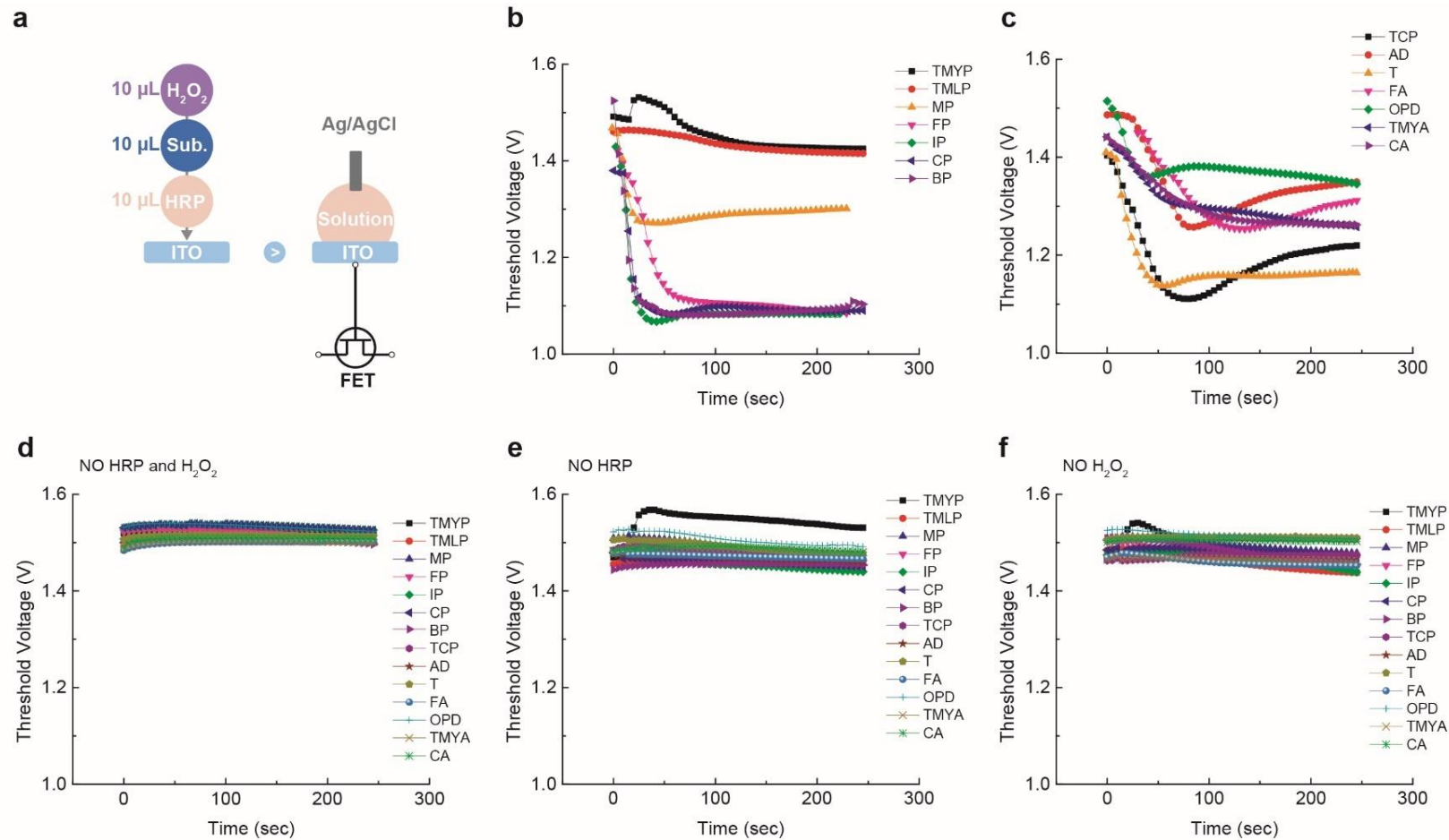


Figure S4. Screening of substrates for REEA signal. (a) Schematic of solution tests for the RGFET setup. 10 μ L each of H_2O_2 , substrate, and HRP solution was placed on the ITO surface, and an Ag/AgCl reference electrode was connected to the solution. (b) Representative V_{th} shifting trend over time for each 10 mM TMYP, TMLP, MP, FP, IP, CP, and BP with HRP (1 $\mu\text{g}/\text{mL}$) and H_2O_2 (5 mM). (c) Representative V_{th} shifting trend over time for each 10 mM TCP, AD, T, FA, OPD, TMYA, and CA with HRP (1 $\mu\text{g}/\text{mL}$) and H_2O_2 (5 mM). (d) Representative V_{th} shifting trend over time for each substrate solution (10 mM) without HRP and H_2O_2 . (e) Representative V_{th} shifting trend over time for each substrate solution (10 mM) with H_2O_2 (5 mM) and without HRP. (f) Representative V_{th} shifting trend over time for each substrate solution (10 mM) with HRP (1 $\mu\text{g}/\text{mL}$) and without H_2O_2 .

Table S2. Simulation for REEA. DFT-calculated enthalpies, Gibbs free energies and pKa values. The density functional theory (DFT) simulation is conducted using Gaussian 16.C.01. The functional is wB97X-D. Basis set is cc-pVDZ for C, H, O, N, F, Cl and LANL2DZ for Br and I. The solvation status is set to be SMD implicit solvent model with no explicit water molecules. For estimating the pKa for phenol-type compounds (TMYP to TCP), the computational method is based on Bishnu's study¹ by standard free energy in **eq. 1**. For estimating the pKa for amino group containing compounds (AD to CA), the computational method is based on the study by Jacinto et al.² to calculate pK_b (=14-pKa) with the surface electrostatic potential ($V_{S,min}$) illustrated by **eq. 2**. The setting using MultiWFN³ is kept the same with isodensity value of 0.001 a.u. For estimating the enthalpy and Gibbs free energy values of oxidization by hydrogen peroxide, the solvation energies of Br⁻, Cl⁻, F⁻ and I⁻ are based on previously reported experimental values^{4,5}.

$$(e \ q. 1) \ pK_a = \frac{G_{sol,RO}^* - G_{sol,H^+}^* - G_{sol,ROH}^*}{2.303RT}$$

$$(e \ q. 2) \ pK_b = 0.4592V_{S,min} + 24.5880$$

Chemical name	DFT-calculated enthalpy change per H ⁺ released (kcal mol ⁻¹)	DFT-calculated Gibbs free energy change per H ⁺ released (kcal mol ⁻¹)	DFT-calculated pKa
2,4,6-Trimethoxyphenol (TMYP)	90.49	86.33	13.69
2,4,6-Trimethylphenol (TMLP)	112.19	108.21	11.01
4-fluorophenol (FP)	-5.15	-13.89	10.81
4-Iodophenol (IP)	-53.78	-65.11	9.32
4-Chlorophenol (CP)	-43.96	-54.22	9.40
4-Bromophenol (BP)	-52.64	-64.15	9.28
2,4,6-Trichlorophenol (TCP)	-44.58	-54.66	2.49
p-Anisidine (AD)	105.98	107.20	6.33
p-Toluidine (T)	107.41	109.59	5.76
2,4,6-Trimethylaniline (TMYA)	108.56	108.37	6.56

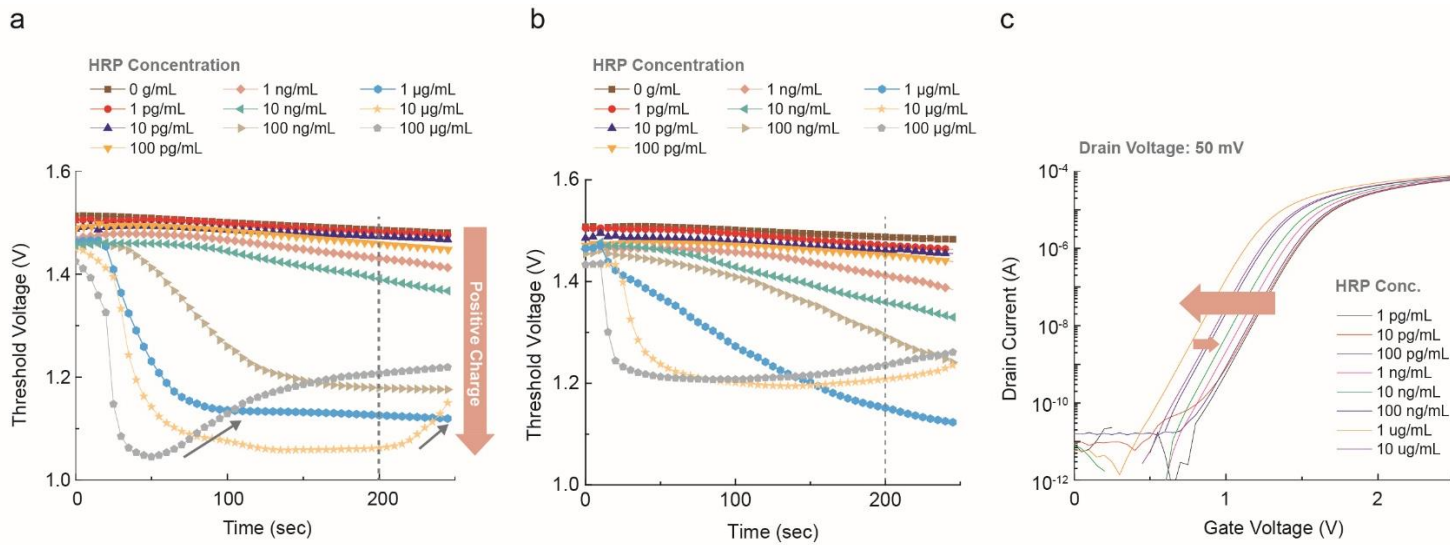


Figure S5. REEA signal depending on HRP concentration. Representative V_{th} shifts over time for varying HRP concentrations in the presence of FP (10 mM) and H_2O_2 (5 mM), diluted in (a) 1X PBS and (b) plasma samples. The V_{th} values presented in Figure 2e were taken at 200 seconds. (c) Representative transfer curves from the final cycle of 50 measurements at different HRP concentrations in the presence of FP (10 mM) and H_2O_2 (5 mM), diluted in plasma samples. The transfer curves exhibit parallel shifts during the HRP-substrate reaction, without changes in shape, even in plasma samples. This indicates that the surface potential changes are specifically caused by the HRP-substrate reaction, with insignificant interference or non-specific signaling.

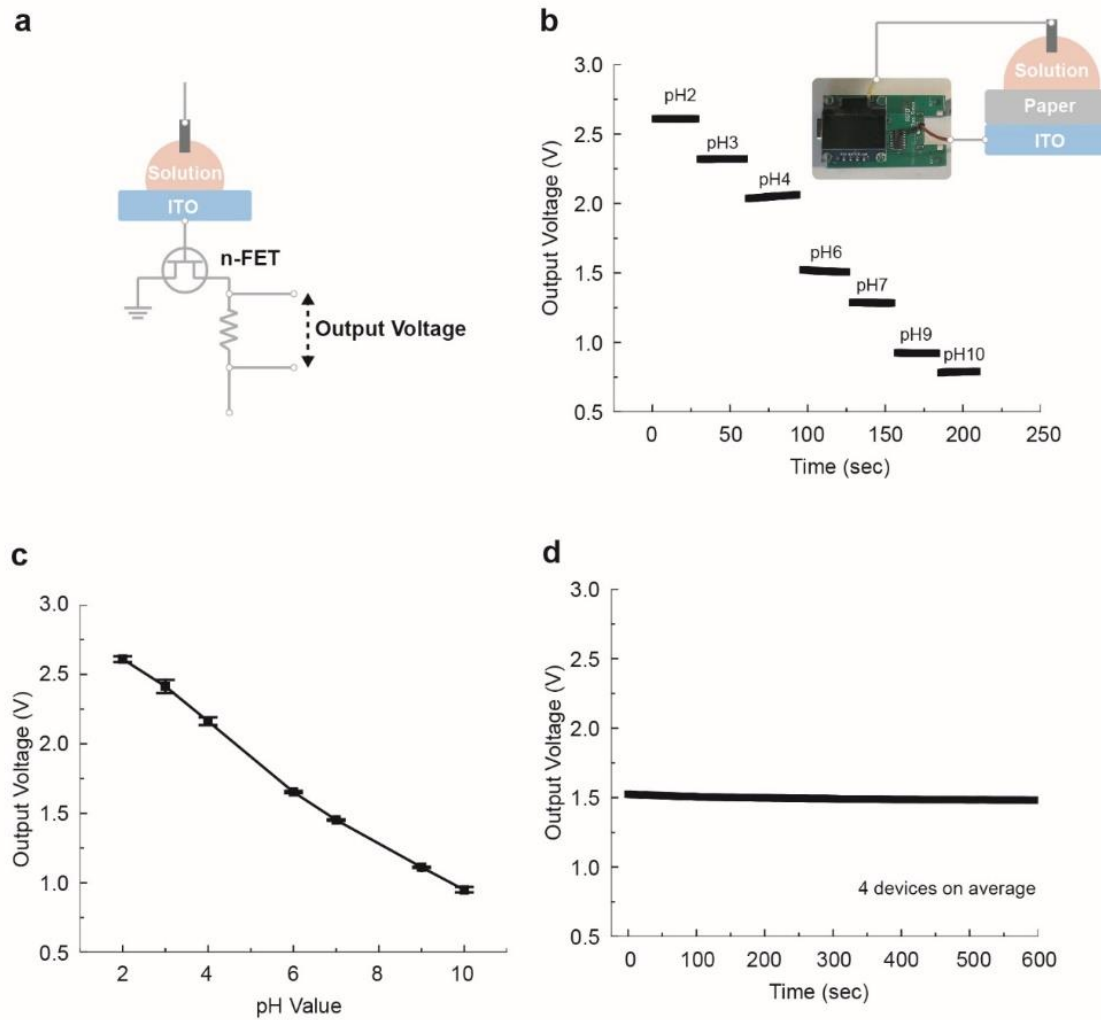


Figure S6. pH sensitivity of RGFET at handheld device. (a) A schematic of the detection system of the handheld device for measurement, (b) Representative real-time V_{out} responses of the handheld device to different pH solutions on the bare ITO in a range from pH 2 to pH 10, (c) pH sensitivity of 212 mV/pH with 99.4% linearity measured over 6 different ITO devices, and (d) drift properties of different ITO measured at pH 6 solution by the handheld device.

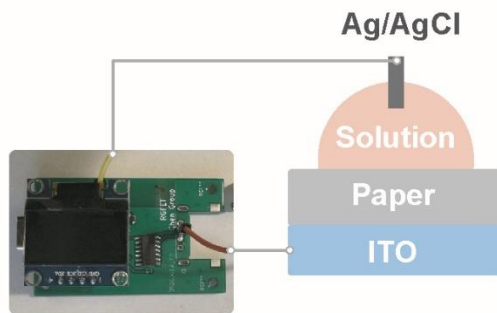
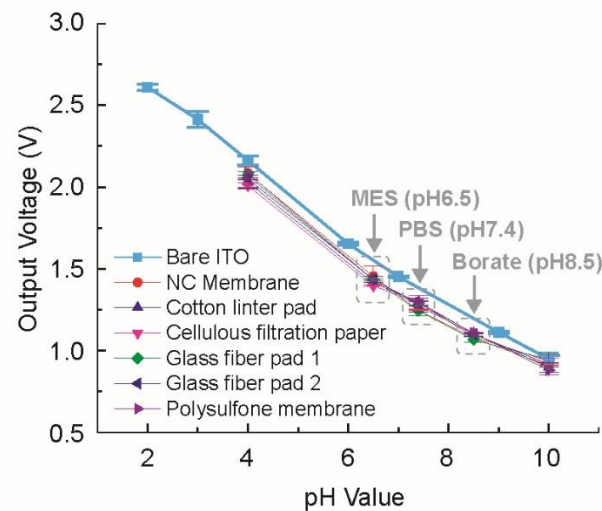
a**b**

Figure S7. Interference tests from different paper materials (a) Handheld device setup used to evaluate interference effects in the V_{out} signal caused by paper materials between the solution and ITO. To facilitate the integration of the LFA system with the handheld FET reader, potential pH detection interferences by various paper materials were examined. (b) V_{out} of ITO measured using different buffer solutions, including standard pH 4 and pH 10 solutions, MES, PBS, and borate, injected on top of various paper materials: nitrocellulose (NC) membrane (Hi-Flow™ Plus 135, MiliporeSigma), cotton linter pad (CF7, Cytiva), cellulous filtration paper (Whatman Grade 1, Cytiva), glass fiber pad 1 (Standard 17, Cytiva), glass fiber pad 2 (PSP60, Axiflow), and polysulfone membrane (MMM, Cytiva). The results showed that the V_{out} readings from these paper-ITO stacks closely matched those taken directly from the ITO surface, suggesting minimal interference from the paper materials. This also demonstrates that the V_{out} signal is only specific to the pH of the buffer solution regardless of the type of paper material between the ITO and the solution.

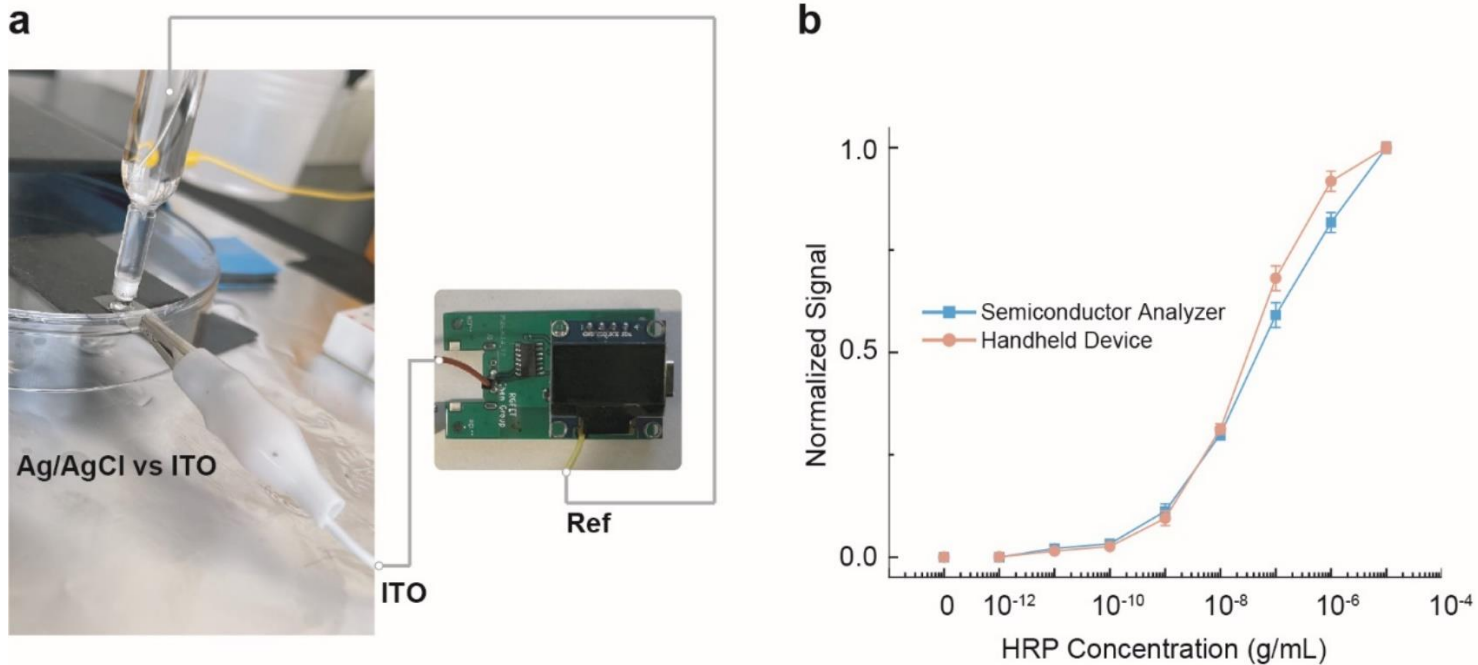


Figure S8. Performance comparison of RGFET measured by a semiconductor analyzer and at a handheld device. (a) Handheld device setup used to compare detection performance between a semiconductor analyzer and the handheld device system. Both sensory modalities utilized identical remote-gate system measurement setups (i.e., Ag/AgCl and ITO) but diverged in the analyzer employed: the semiconductor analyzer and the handheld device. (b) Normalized electrical signals of the handheld device and semiconductor analyzer plotted against HRP concentrations, while maintaining constant H_2O_2 (5 mM) and FP (10 mM) concentrations for all measurements. The V_{out} from the handheld device and V_{th} from the semiconductor analyzer were normalized for comparison.

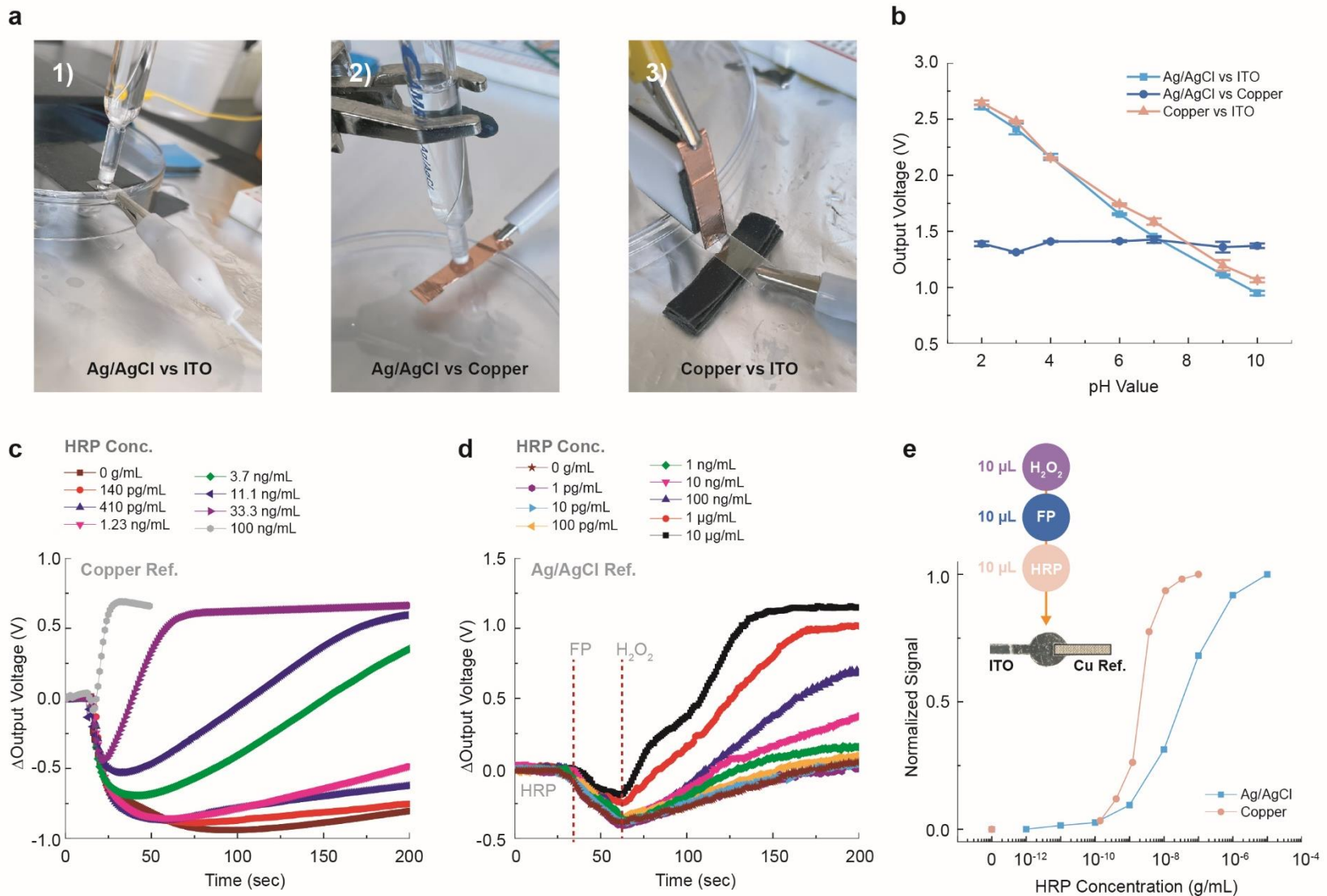


Figure S9. Reference electrode tests in REEA signal. (a) Image of the measurement system illustrating three configurations: 1) Ag/AgCl reference with ITO as the sensing electrode, 2) Ag/AgCl reference with copper as the sensing electrode, and 3) copper reference electrode with ITO as the sensing electrode. (b) V_{out} response to pH solutions for each configuration, measured using the handheld device. No pH sensitivity was observed when the copper electrode was used as the sensing electrode with the Ag/AgCl reference. Representative real-time V_{out} responses for the reaction

between FP and varying HRP concentrations (0 to 100 ng/mL) on the bare ITO were measured using (c) a copper reference electrode and (d) an Ag/AgCl reference electrode. In both cases, 5 mM H_2O_2 and 10 mM FP were used. (e) Normalized V_{out} signals from panels (c) and (d) versus HRP concentration; the ΔV_{out} values for panel (e) were calculated from the ΔV_{out} at 200 seconds in panels (c) and (d). The inset in panel (e) shows a photo of the ITO and copper electrode setup for monitoring the HRP-FP reaction.

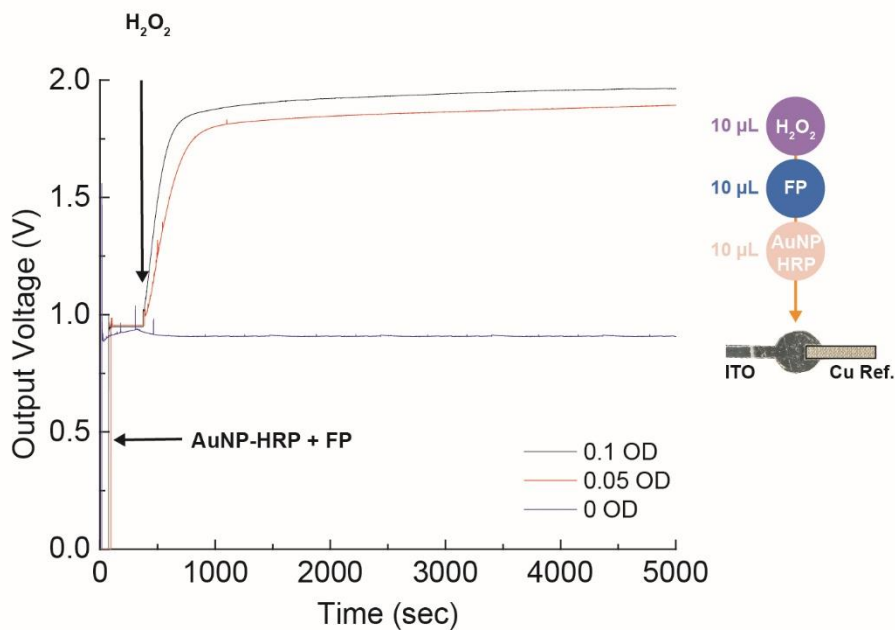


Figure S10. REEA signal of AuNP-HRP-E2 conjugate tested in solution phase. Representative raw V_{out} curves of AuNP-HRP conjugates and the substrate reaction, measured using an ITO-Cu electrode and a handheld reader device. 10 μL of each AuNP-HRP conjugate with varying concentrations (0, 0.05, and 0.1 OD) and 5 mM FP were added sequentially on the electrode, and the baseline was monitored for 600 s. Subsequently, 10 μL of 10 mM H_2O_2 solution was added to the solution in the electrode chamber, and the signal was monitored for up to 5000 s. Once the V_{out} reached a specific value corresponding to the AuNP-HRP concentration, the signal remained stable with no observable drift over 5000 s.

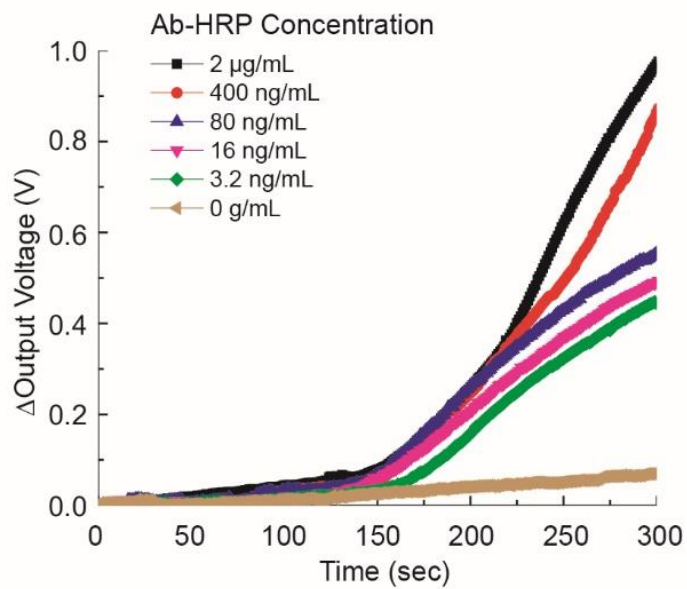


Figure S11. REEA signal tested on paper material. Representative real-time V_{out} responses of different paper fluidics cartridges functionalized with varying concentrations of secondary antibody-HRP conjugation, ranging from 0 to 2 μ g/mL, on the sensing zone after loading the FP (5 mM) and H_2O_2 solution (10 mM). ΔV_{out} for Figure 3a was recorded at 250 seconds.

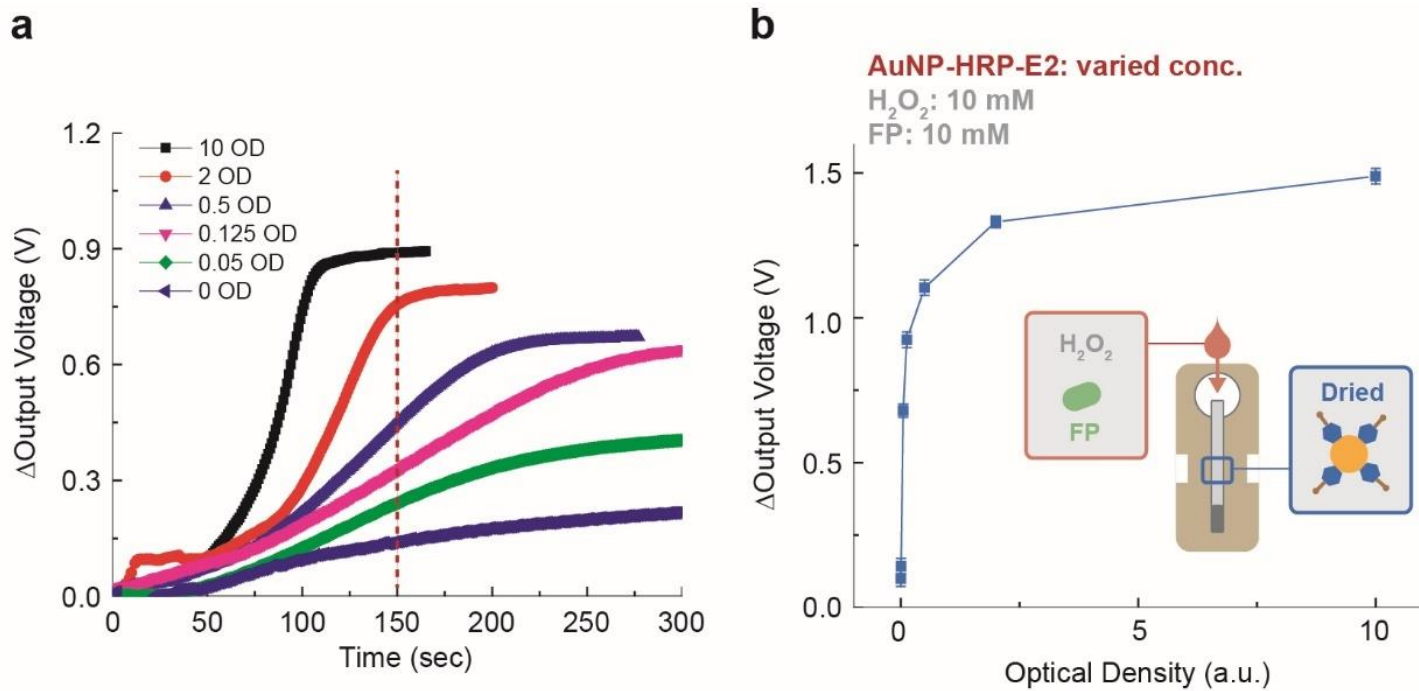


Figure S12. Titration curves of the REEA signal depending on the concentration of AuNP-HRP-E2 conjugate. (a) Representative real-time V_{out} responses of paper fluidics cartridges functionalized with varying concentrations of AuNP-HRP-E2 conjugate, ranging from 0 to 10 OD, dried on the sensing zone of paper fluidics after loading the FP solution. (b) ΔV_{out} for each concentration of AuNP conjugate recorded at 150 seconds.

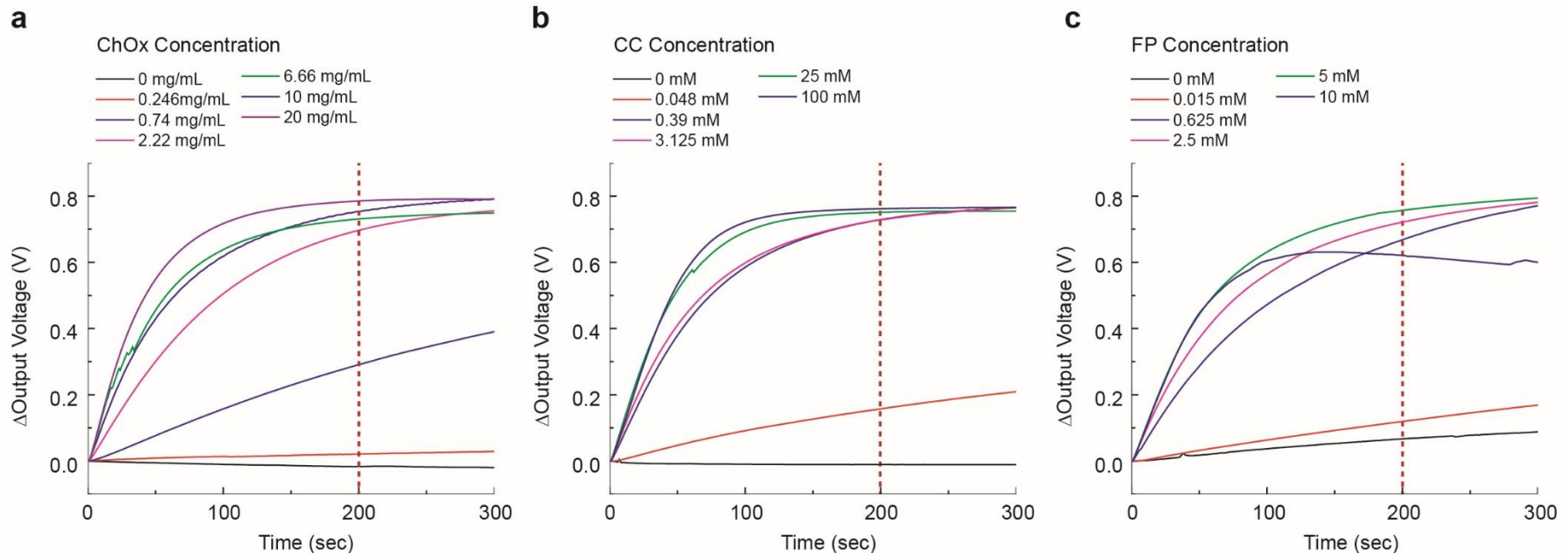


Figure S13. Optimization of REEA components. (a) Representative real-time V_{out} responses of paper fluidics dried with varying concentrations of ChOx (for testing solution: AuNP-HRP-E2 at 0.05 OD, CC at 25 mM, and FP at 5 mM). (b) Representative real-time V_{out} responses of paper fluidics dried with 10 mg/mL ChOx in response to different CC concentrations (for testing solution: AuNP-HRP-E2 at 0.05 OD, and FP at 5 mM). (c) Representative real-time V_{out} responses of paper fluidics dried with 10 mg/mL ChOx in response to varying FP concentrations (for testing solution: AuNP-HRP-E2 at 0.05 OD, and CC at 25 mM).

Table S3. Optimization of running buffer components. Impact of various surfactants and other reagents on capture efficiency, signal window, proton generation, and baseline uniformity in a paper fluidics system. This table summarizes the effects of different reagents when mixed into 2% BSA in 1X PBS solution on the assay's performance. All percentage changes are reported relative to each control. To screen the surfactant group, each surfactant was mixed at a concentration of 0.2% (v/v) in 2% BSA. Stabilizers were also mixed with 2% BSA according to the concentrations listed in the table. All paper fluidics used in Table S3 were dried with 1 mg/mL E2 antibody. E2 capture efficiency was assessed by the colorimetric signal and is expressed as percentages relative to the control (optical signal obtained from 1 OD AuNP-HRP-E2 conjugate solution in 2% BSA), with -100% indicating no optical signal and positive values indicating stronger optical signals than the control; E2 antibody dried on paper fluidics system capture AuNP-HRP-E2 conjugate. The signal resolution was also assessed by the colorimetric signal, where the control for the signal resolution is defined as the difference in optical signal between the 1 OD AuNP-HRP-E2 conjugate solution diluted in 2% BSA (i.e., no free E2) and the same solution with 1 ng/mL spiked E2. Proton generation was assessed by HRP-FP reaction for ChOx automated system and is expressed as a percentage relative to the control (0.05 OD AuNP-HRP-E2 conjugate solution in 2% BSA, 10 mM FP, and 25 mM CC). The results demonstrate that surfactants such as TX-100, Tween 20, and Aerosol® OT significantly decreased capture efficiency and signal window, while reagents like IGEPAL® CA610 and BRIJ® 98 showed improved proton generation. Notably, 2.5% Polyvinylpyrrolidone and 1% sucrose also influenced the signal window and baseline, while some reagents like acetonitrile led to complete loss of proton generation. Additionally, the coefficient of variation (CV) for the baseline of the REEA signal obtained by the handheld device was compared across different reagents in the same table to evaluate baseline uniformity.

No	Reagents	Capture efficiency	Signal resolution	Proton generation	Baseline	
					CV (%)	% Bias
1	Control (2% BSA in 1X PBS)	0.00%	0.00%	0.00%	16.94%	19.03%
2	Surfactants	TX-100	-100.00%	-100.00%	-44.05%	3.68%
3		Tween 20	-60.86%	-100.00%	-20.77%	7.66%
4		Surfactant 10G	-91.55%	-12.92%	-6.88%	5.39%
5		Chemal LA-9	-26.17%	-25.05%	-22.96%	0.64%
6		Aerosol® OT	13.44%	-67.48%	-73.37%	6.32%
7		Pluronic® L64	-25.80%	-67.31%	-56.09%	3.17%
						2.73%

8	IGEPAL® CA610	21.83%	-12.93%	31.06%	3.04%	-3.99%
9	Pluronic® F127	-68.93%	-57.17%	-45.05%	6.37%	1.61%
10	Pluronic® F68	-1.47%	-67.34%	41.81%	0.70%	-4.12%
11	BRIJ® 98	2.24%	-58.50%	135.44%	2.45%	-4.86%
12	Triton® X-305	-100.00%	45.62%	39.10%	0.51%	-0.25%
13	BRIJ® 35	3.11%	-58.10%	85.59%	2.20%	-7.15%
14	Triton® X-45	-83.70%	-75.03%	-47.91%	5.13%	1.97%
15	Tween® 80	55.80%	-56.18%	-18.92%	0.90%	3.73%
16	Tergitol®	-97.59%	70.95%	-26.11%	0.50%	-8.17%
17	Silwet® L7600	27.31%	-55.92%	83.48%	0.49%	-8.44%
18	Synperonic® F108	-67.82%	1.72%	-44.95%	0.90%	-5.71%
19	Cremophor® EL	45.77%	-40.18%	-4.46%	7.74%	-4.97%
20	Tween® 60	49.60%	-68.37%	10.41%	3.19%	-9.88%
21	Merpol® A	31.90%	-34.72%	-72.68%	0.47%	-7.00%
22	Benzalkonium	-79.62%	-100.00%	-73.63%	0.32%	-9.95%
23	Tetronic® 90R4	21.00%	-59.26%	-66.82%	0.36%	-2.05%
24	2,4,7,9-Tetramethyl-5-decindiol	3.65%	-64.66%	-19.23%	5.13%	-17.95%
25	2.5% Polyvinylpyrrolidone	-8.94%	66.49%	-17.06%	2.33%	5.95%
26	1% Sucrose	-0.39%	23.75%	Not measured	6.57%	5.85%
27	5% EtOH	-0.85%	-17.73%	-29.86%	6.86%	2.24%
28	5% IPA	5.75%	-42.62%	-42.37%	3.11%	3.24%
29	Stabilizers	1% Polyvinyl Alcohol	-13.41%	-46.37%	Not measured	7.48%
30		1% Polyethylene glycol	-5.35%	-61.18%	-50.99%	1.66%
31		10% Acetonitrile	-7.75%	-6.63%	-100.00%	2.25%
32		1% Trehalose	-5.57%	30.45%	Not measured	5.00%
						1.45%

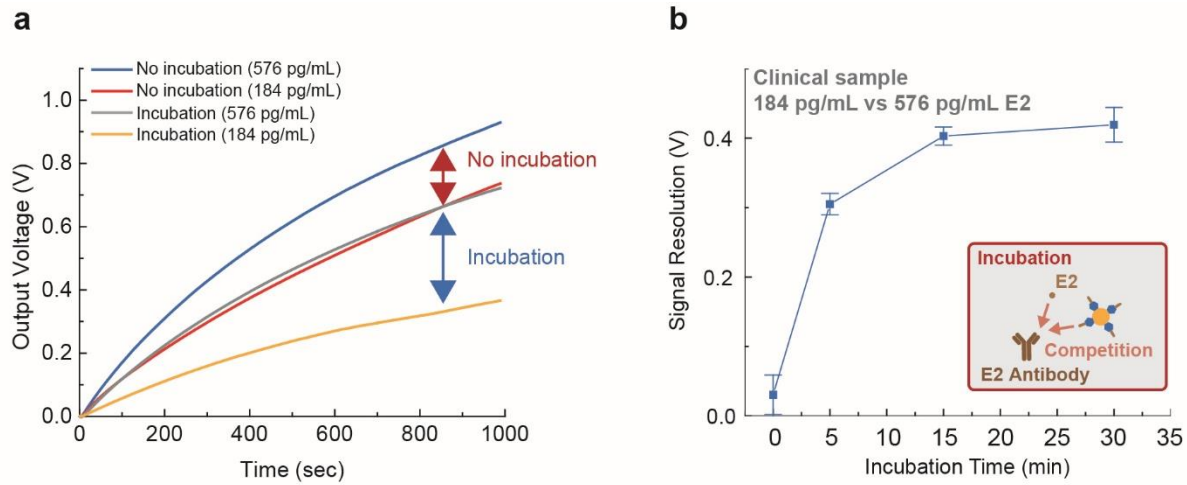


Figure S14. Incubation time effect. (a) Representative real-time V_{out} responses were measured from testing solutions containing 10 $\mu\text{g/mL}$ E2 antibodies, 0.1 OD AuNP-HRP-E2 conjugate, 10 mM FP, and 25 mM CC, using clinical plasma samples with E2 concentrations of 184 pg/mL and 576 pg/mL. The testing samples were incubated for 15 minutes prior to injection. Without the incubation step, the difference in signals between the two samples was insignificant. (b) Signal resolution, affected by incubation time, is obtained as the difference in output voltage between 184 pg/mL and 576 pg/mL, measured at 1,500 seconds. This ensures that the value is captured at saturated output voltages for each case, without the influence of signal changes caused by measurement time, as shown in Figure S15.

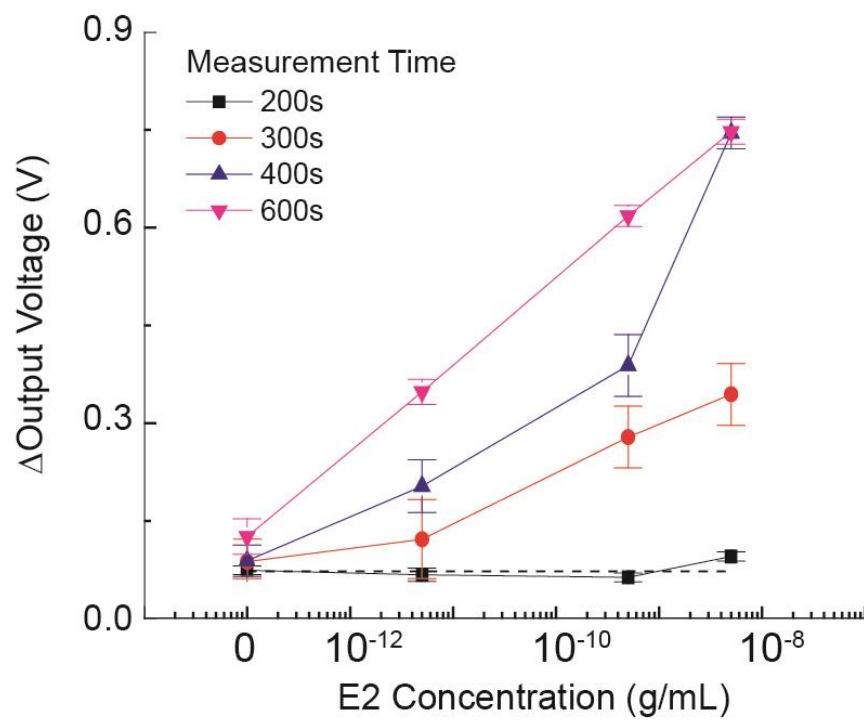


Figure S15. Signal resolution depending on measurement time. ΔV_{out} response over varying measurement times for E2-spiked samples, ranging from 5 pg/mL to 50 ng/mL, measured using the incubation method.

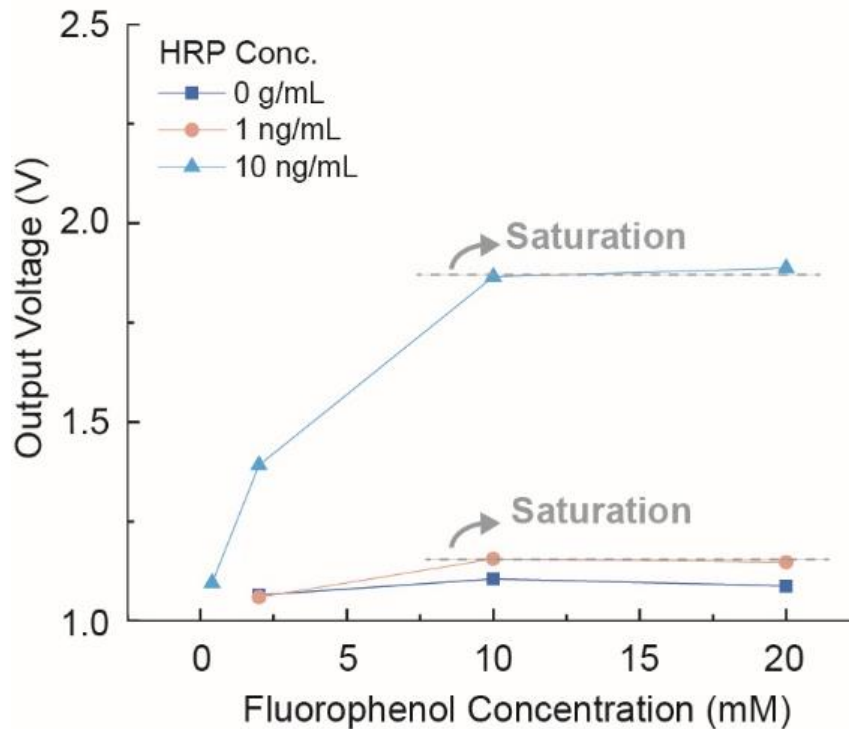


Figure S16. Optimization of FP concentration for REEA. V_{out} change of the handheld device to FP concentration on the bare ITO with different HRP concentrations of 0, 1, and 10 ng/mL with fixed H_2O_2 (5 mM). These measurements were taken on a bare ITO surface using the standard Ag/AgCl reference electrode. Optimal substrate concentration of FP for the REEA was found to be 10 mM while FP concentrations exceeding 10 mM resulted in saturated signals. Consequently, an FP concentration of 10 mM was selected for all further experiments, ensuring consistency and accuracy in the REEA process.

References for Supporting information

1. Thapa, B., and Schlegel, H.B. (2017). Improved pK(a) Prediction of Substituted Alcohols, Phenols, and Hydroperoxides in Aqueous Medium Using Density Functional Theory and a Cluster-Continuum Solvation Model. *J. Phys. Chem. A* **121**, 4698-4706. 10.1021/acs.jpca.7b03907.
2. Sandoval-Lira, J., Mondragon-Solorzano, G., Lugo-Fuentes, L.I., and Barroso-Flores, J. (2020). Accurate Estimation of pK(b) Values for Amino Groups from Surface Electrostatic Potential ($V(S,\text{min})$) Calculations: The Isoelectric Points of Amino Acids as a Case Study. *J. Chem. Inf. Model* **60**, 1445-1452. 10.1021/acs.jcim.9b01173.
3. Lu, T., and Chen, F. (2012). Multiwfn: a multifunctional wavefunction analyzer. *J. Comput. Chem.* **33**, 580-592. 10.1002/jcc.22885.
4. Tissandier, M.D., Cowen, K.A., Feng, W.Y., Gundlach, E., Cohen, M.H., Earhart, A.D., Coe, J.V., and Tuttle, T.R. (1998). The proton's absolute aqueous enthalpy and Gibbs free energy of solvation from cluster-ion solvation data. *J. Phys. Chem. A* **102**, 7787-7794. 10.1021/jp982638r.
5. Fawcett, W.R. (1999). Thermodynamic parameters for the solvation of monatomic ions in water. *J. Phys. Chem. B* **103**, 11181-11185. 10.1021/jp991802n